

2.06 Theory and Practice – Thermodynamics, Equations of State, Elasticity, and Phase Transitions of Minerals at High Pressures and Temperatures

A. R. Oganov, ETH Zurich, Zurich, Switzerland

© 2007 Elsevier B.V. All rights reserved.

| | | |
|-------------------|--|-----|
| 2.06.1 | Thermodynamics of Crystals | 122 |
| 2.06.1.1 | Thermodynamic Potentials | 122 |
| 2.06.1.2 | Differential Relations | 122 |
| 2.06.1.3 | Partition Function | 123 |
| 2.06.1.4 | Harmonic Approximation | 124 |
| 2.06.1.4.1 | Debye model | 125 |
| 2.06.1.4.2 | General harmonic potential | 126 |
| 2.06.1.5 | Quantum Effects in Thermodynamics | 127 |
| 2.06.1.6 | Thermodynamic Perturbation Theory | 128 |
| 2.06.1.7 | Quasiharmonic Approximation | 129 |
| 2.06.1.8 | Beyond the QHA | 129 |
| 2.06.2 | Equations of State and Elasticity | 131 |
| 2.06.2.1 | Equations of State | 131 |
| 2.06.2.1.1 | Mie–Grüneisen EOS | 131 |
| 2.06.2.1.2 | Analytical static EOS | 132 |
| 2.06.2.1.3 | Anharmonicity in static EOS | 134 |
| 2.06.2.1.4 | EOS, internal strain, and phase transitions | 134 |
| 2.06.2.2 | Elastic Constants | 135 |
| 2.06.2.2.1 | Cauchy relations | 138 |
| 2.06.2.2.2 | Mechanical stability | 139 |
| 2.06.2.2.3 | Birch's law and effects of temperature on the elastic constants | 139 |
| 2.06.2.2.4 | Elastic anisotropy in the Earth's interior | 140 |
| 2.06.3 | Phase Transitions of Crystals | 140 |
| 2.06.3.1 | Classifications of Phase Transitions | 140 |
| 2.06.3.2 | First-Order Phase Transitions | 141 |
| 2.06.3.3 | Landau Theory of First- and Second-Order Transitions | 141 |
| 2.06.3.4 | Shortcomings of Landau Theory | 142 |
| 2.06.3.5 | Ginzburg–Landau Theory | 143 |
| 2.06.3.6 | Ising Spin Model | 144 |
| 2.06.3.7 | Mean-Field Treatment of Order–Disorder Phenomena | 145 |
| 2.06.3.8 | Isosymmetric Transitions | 145 |
| 2.06.3.9 | Transitions with Group–Subgroup Relations | 146 |
| 2.06.3.10 | Pressure-Induced Amorphization | 146 |
| 2.06.4 | A Few Examples of the Discussed Concepts | 147 |
| 2.06.4.1 | Temperature Profile of the Earth's Lower Mantle and Core | 147 |
| 2.06.4.2 | Polytypism of MgSiO ₃ Post-Perovskite and Anisotropy of the Earth's D'' layer | 147 |
| 2.06.4.3 | Spin Transition in (Mg, Fe)O Magnesio-wüstite | 148 |
| References | | 149 |

2.06.1 Thermodynamics of Crystals

Thermodynamics provides the general basis for the theory of structure and properties of matter. This chapter presents only as much thermodynamics as needed for good comprehension of geophysics, and at a relatively advanced level. For further reading the reader is referred to Landau and Lifshitz (1980), Chandler (1987), Wallace (1998), and Bowley and Sánchez (1999).

2.06.1.1 Thermodynamic Potentials

If one considers some system (e.g., a crystal structure) at temperature $T = 0$ K and pressure $P = 0$, the equilibrium state of that system corresponds to the minimum of the internal energy E :

$$E \rightarrow \min \quad [1]$$

that is, any changes (e.g., atomic displacements) would result in an increase of energy. The internal energy itself is a sum of the potential and kinetic energies of all the particles (nuclei, electrons) in the system.

The principle [1] is valid in only two situations: (1) at $T = 0$ K, $P = 0$, and (2) at constant V (volume) and S (entropy), that is, if we impose constraints of constant S, V , the system will adopt the lowest-energy state. Principle [1] is a special case of a more general principle that the thermodynamic potential W describing the system be minimum at equilibrium:

$$W \rightarrow \min \quad [2]$$

As already mentioned, at constant V, S : $W_{V,S} = E \rightarrow \min$.

At constant P, S , the appropriate thermodynamic potential is the enthalpy H :

$$W_{P,S} = H = E + PV \rightarrow \min \quad [3]$$

At constant V, T , the Helmholtz free energy F is the thermodynamic potential:

$$W_{V,T} = F = E - TS \rightarrow \min \quad [4]$$

At constant P, T (the most frequent practical situation), the relevant thermodynamic potential is the Gibbs free energy G :

$$W_{P,T} = G = E + PV - TS \rightarrow \min \quad [5]$$

The minimum condition implies that

$$\frac{\partial W}{\partial x_i} = 0 \quad [6]$$

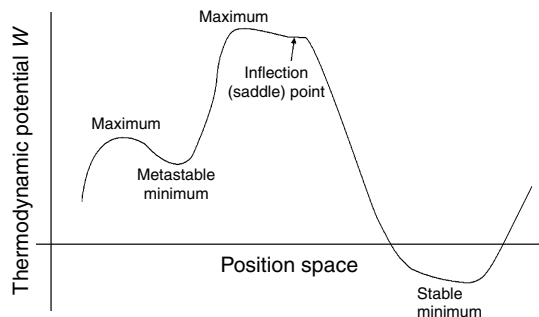


Figure 1 Extrema and saddle points in a one-dimensional representation of the (free) energy surface.

However, this condition is also satisfied for maxima of the thermodynamic potential, and for saddle points (Figure 1). To exclude saddle points and maxima, one has to make sure that the matrix of second derivatives of W with respect to all the degrees of freedom (in case of a crystal structure, with respect to atomic coordinates and lattice parameters):

$$H_{ij} = \frac{\partial^2 W}{\partial x_i \partial x_j} \quad [7]$$

be positive definite:

$$\det \mathbf{H}_{ij} > 0 \quad [8]$$

Still, there may be a large (or infinite) number of minima. The equilibrium state corresponds to the lowest minimum of W (the global minimum), whereas all the other minima are called local and correspond to metastable states. Local minima have the property of stability to an infinitesimal displacement (after any such displacement the system returns to the initial state), but one can always find a sufficiently large energy fluctuation that will irreversibly destroy the metastable state.

2.06.1.2 Differential Relations

From the first law of thermodynamics one has

$$dE = -P dV + T dS \quad [9]$$

Applying Legendre transformations, the following relations can be obtained:

$$dH = V dP + T dS \quad [10]$$

$$dF = -P dV - S dT \quad [11]$$

$$dG = V dP - S dT \quad [12]$$

When there is thermodynamic equilibrium between two phases (denoted 1 and 2) at given P and T ,

$G_1 = G_2$. Moving along the two-phase equilibrium line in P - T space requires $dG_1 = dG_2$, that is,

$$\Delta V dP - \Delta S dT = 0 \quad [13]$$

or, in a different form,

$$\frac{dP}{dT} = \frac{\Delta S}{\Delta V} \quad [14]$$

This is the famous Clausius–Clapeyron equation.

Using eqns [9]–[12], one can express various thermodynamic parameters:

$$P = -\left(\frac{\partial E}{\partial V}\right)_S = -\left(\frac{\partial F}{\partial V}\right)_T \quad [15]$$

$$V = \left(\frac{\partial H}{\partial P}\right)_S = \left(\frac{\partial G}{\partial P}\right)_T \quad [16]$$

$$T = \left(\frac{\partial E}{\partial S}\right)_V = \left(\frac{\partial H}{\partial S}\right)_P \quad [17]$$

$$S = -\left(\frac{\partial F}{\partial V}\right)_S = -\left(\frac{\partial G}{\partial T}\right)_P \quad [18]$$

Taking second derivatives, Maxwell relations are obtained (see, e.g., Poirier (2000)):

$$\left(\frac{\partial S}{\partial P}\right)_T = -\left(\frac{\partial V}{\partial T}\right)_P \quad [19]$$

$$\left(\frac{\partial S}{\partial V}\right)_T = \left(\frac{\partial P}{\partial T}\right)_V \quad [20]$$

$$\left(\frac{\partial T}{\partial P}\right)_S = \left(\frac{\partial V}{\partial S}\right)_P \quad [21]$$

$$\left(\frac{\partial T}{\partial V}\right)_S = -\left(\frac{\partial P}{\partial S}\right)_V \quad [22]$$

Using the Maxwell relations, a number of important thermodynamic relations are derived, for example,

$$\left(\frac{\partial S}{\partial V}\right)_T = \alpha K_T \quad [23]$$

$$\left(\frac{\partial S}{\partial V}\right)_P = \frac{C_p}{\alpha V T} \quad [24]$$

$$\left(\frac{\partial S}{\partial P}\right)_T = -\alpha V \quad [25]$$

$$\left(\frac{\partial T}{\partial P}\right)_S = \frac{\alpha V T}{C_p} \quad [26]$$

$$\left(\frac{\partial V}{\partial T}\right)_S = -\frac{C_p}{\alpha K_S T} \quad [27]$$

$$\left(\frac{\partial P}{\partial T}\right)_V = \alpha K_T \quad [28]$$

In eqns [23]–[28] we used thermal expansion

$$\alpha = \frac{1}{V} \left(\frac{\partial V}{\partial T}\right)_P \quad [29]$$

isothermal bulk modulus

$$K_T = -\frac{1}{V} \left(\frac{\partial V}{\partial P}\right)_S \quad [30]$$

and isobaric heat capacity

$$C_p = \left(\frac{\partial E}{\partial T}\right)_P \quad [31]$$

We note, on passing, that the bulk modulus and the heat capacity depend on the conditions of measurement. There are general thermodynamic equations relating the heat capacity at constant pressure (isobaric) and constant volume (isochoric):

$$C_p = C_V \left(1 + \frac{\alpha^2 K_T V}{C_V}\right) \quad [32]$$

and bulk modulus at constant temperature (isothermal) and at constant entropy (adiabatic):

$$K_S = K_T \left(1 + \frac{\alpha^2 K_T V}{C_p}\right) \quad [33]$$

The most interesting of eqns [23]–[28] are eqn [26], describing the increase of the temperature of a body on adiabatic compression (e.g., in shock waves, and also inside rapidly convecting parts of planets), and eqn [28], describing thermal pressure. These equations are important for thermal equations of state and for calculating the temperature distributions inside planets.

2.06.1.3 Partition Function

Let us consider a system with energy levels E_i corresponding to the ground state and all the excited states. The probability to find the system in the i th state is proportional to $e^{-\beta E_i}$, where $\beta = 1/(k_B T)$ (k_B is the Boltzmann constant).

More rigorously, this probability p_i is given as

$$p_i = \frac{e^{-\beta E_i}}{\sum_i e^{-\beta E_i}} \quad [34]$$

The denominator of this equation is called the partition function Z :

$$Z = \sum_i e^{-\beta E_i} \quad [35]$$

where the summation is carried out over all discrete energy levels of the system. The partition function is

much more than a mere normalization factor; it plays a fundamental role in statistical physics, providing a link between the microscopic energetics and the macroscopic thermodynamics. Once Z is known, all thermodynamic properties can be obtained straightforwardly (e.g., Landau and Lifshitz, 1980). For instance, the internal energy

$$E = \sum_i p_i E_i = \frac{\sum_i E_i e^{-\beta E_i}}{Z} = -\frac{1}{Z} \left(\frac{\partial Z}{\partial \beta} \right)_V$$

$$= - \left(\frac{\partial \ln Z}{\partial \beta} \right)_V \quad [36]$$

From this one can derive a very important expression for the Helmholtz free energy

$$F = -\frac{1}{\beta} \ln Z = -k_B T \ln Z \quad [37]$$

entropy

$$S = K_B \ln Z - \frac{k_B \beta}{Z} \left(\frac{\partial Z}{\partial \beta} \right)_V \quad [38]$$

and the heat capacity at constant volume (From eqn [39] one can derive (see Dove, 2003) the following important formula: $C_V = K_B \beta^2 (\langle E^2 \rangle - \langle E \rangle^2)$):

$$C_V = -\frac{k_B \beta^2}{Z^2} \left(\frac{\partial Z}{\partial \beta} \right)_V^2 + \frac{k_B \beta^2}{Z} \left(\frac{\partial^2 Z}{\partial \beta^2} \right)_V \quad [39]$$

Unfortunately, in many real-life cases it is practically impossible to obtain all the energy levels – neither experimentally nor theoretically, and therefore the partition function cannot be calculated exactly. However, for some simplified models it is possible to find the energy levels and estimate the partition function, which can then be used to calculate thermodynamic properties.

Below we consider the harmonic approximation, which plays a key role in the theory of thermodynamic properties of crystals. It gives a first approximation to the distribution of the energy levels E_i , which is usually accurate for the most-populated lowest excited vibrational levels. The effects not accounted for by this simplified picture can often be included as additive corrections to the harmonic results.

2.06.1.4 Harmonic Approximation

The harmonic oscillator is a simple model system where the potential energy (U) is a quadratic

function of the displacement x from equilibrium, for example, for a simple diatomic molecule

$$U(x) = U_0 + \frac{1}{2} k x^2 \quad [40]$$

where U_0 is the reference energy and k is the force constant.

The energy levels of the harmonic oscillator can be found by solving the Schrödinger equation with the harmonic potential [40]; the result is an infinite set of equi-spaced energy levels:

$$E_n = \left(\frac{1}{2} + n \right) \hbar \omega \quad [41]$$

where \hbar is Planck's constant, ω is the vibrational frequency of the oscillator, and integer n is the quantum number: $n=0$ for the ground state, and $n \geq 1$ for excited states. Energy levels in a true vibrational system are well described by [41] only for the lowest quantum numbers n , but these represent the most populated, and thus the most important vibrational excitations.

A very interesting feature of [41] is that even when $n=0$, that is, when there are no vibrational excitations (at 0 K), there is still a vibrational energy equal to $\hbar\omega/2$. This energy is called zero-point energy and arises from quantum fluctuations related to the Heisenberg uncertainty principle.

With [41] the partition function for the harmonic oscillator is rather simple:

$$Z = \frac{1}{1 - e^{-\hbar\omega/k_B T}} \quad [42]$$

This allows one to calculate thermodynamic functions of a single harmonic oscillator (as was first done by Einstein):

$$E_{\text{vib}}(\omega, T) = \frac{1}{2} \hbar \omega + \frac{\hbar \omega}{\exp(\hbar\omega/k_B T) - 1} \quad [43]$$

$$C_{V,\text{vib}}(\omega, T) = k_B \left(\frac{\hbar \omega}{k_B T} \right)^2 \frac{\exp(\hbar\omega/k_B T)}{(\exp(\hbar\omega/k_B T) - 1)^2} \quad [44]$$

$$S_{\text{vib}}(\omega, T) = -k_B \ln[1 - \exp(-\hbar\omega/k_B T)] + \frac{1}{T} \frac{\hbar \omega}{\exp(\hbar\omega/k_B T) - 1} \quad [45]$$

$$F_{\text{vib}}(\omega, T) = \frac{1}{2} \hbar \omega + k_B T \ln \left[1 - \exp\left(-\frac{\hbar \omega}{k_B T}\right) \right] \quad [46]$$

The first term in [43] is the zero-point energy originating from quantum motion of atoms discussed above. The second, temperature-dependent term gives the thermal energy according to the Bose–Einstein distribution. The thermal energy (or heat

content) gives the energy absorbed by the crystal upon heating from 0 K to the temperature T . In the harmonic approximation, the isochoric C_V and isobaric C_p heat capacities are equal: $C_V = C_p$.

The number of phonons in a crystal containing N atoms in the unit cell is $3N$ (per unit cell). In the harmonic approximation, lattice vibrations do not interact with each other (in other words, propagation of one vibration does not change the energy or momentum of other vibrations), and their contributions to thermodynamic properties are additive. If all of the phonons had the same frequency (the assumption of the Einstein model), then, multiplying the right-hand sides of [43]–[46] by the total number of vibrations $3N$, all thermodynamic properties would be obtained immediately. However, normal mode frequencies form a spectrum (called the phonon spectrum, or phonon density of states $g(\omega)$); and an appropriate generalization [43]–[46] involves integration over all frequencies:

$$\begin{aligned} E_{\text{vib}}(T) &= \int_0^{\omega_{\text{max}}} E_{\text{vib}}(\omega, T)g(\omega)d\omega \\ &= \int_0^{\omega_{\text{max}}} \left(\frac{1}{2}\hbar\omega + \frac{\hbar\omega}{\exp(\hbar\omega/k_B T) - 1} \right) \\ &\quad \times g(\omega)d\omega \end{aligned} \quad [47]$$

$$\begin{aligned} C_{V,\text{vib}}(T) &= \int_0^{\omega_{\text{max}}} C_{V,\text{vib}}(\omega, T)g(\omega)d\omega \\ &= \int_0^{\omega_{\text{max}}} \left(k_B \left(\frac{\hbar\omega}{k_B T} \right)^2 \frac{\exp(\hbar\omega/k_B T)}{(\exp(\hbar\omega/k_B T) - 1)^2} \right) \\ &\quad \times g(\omega)d\omega \end{aligned} \quad [48]$$

$$\begin{aligned} S_{\text{vib}}(T) &= \int_0^{\omega_{\text{max}}} S_{\text{vib}}(\omega, T)g(\omega)d\omega \\ &= \int_0^{\omega_{\text{max}}} \left(-k_B \ln \left[1 - \exp\left(-\frac{\hbar\omega}{k_B T} \right) \right] \right. \\ &\quad \left. + \frac{1}{T} \frac{\hbar\omega}{\exp(\hbar\omega/k_B T) - 1} \right) g(\omega)d\omega \end{aligned} \quad [49]$$

$$\begin{aligned} F_{\text{vib}}(T) &= \int_0^{\omega_{\text{max}}} F_{\text{vib}}(\omega, T) \\ &= \int_0^{\omega_{\text{max}}} \left(\frac{1}{2}\hbar\omega + k_B T \ln \left\{ 1 - \exp\left(-\frac{\hbar\omega}{k_B T} \right) \right\} \right) \\ &\quad \times g(\omega)d\omega \end{aligned} \quad [50]$$

2.06.1.4.1 Debye model

In early works, the phonon density of states $g(\omega)$ had often been simplified using the Debye model. For the

acoustic modes the phonon spectrum can be described, to a first approximation, by a parabolic function:

$$g(\omega) = 9N \left(\frac{\hbar}{k_B \theta_D} \right)^3 \omega^2 \quad [51]$$

truncated at the maximum frequency $\omega_D = (k_B \theta_D)/\hbar$, where θ_D is the Debye temperature.

With this $g(\omega)$ thermodynamic functions take the following form:

$$E_{\text{vib}} = \frac{9}{8} k_B N \theta_D + 3 k_B N T D \left(\frac{\theta_D}{T} \right) \quad [52]$$

$$C_V(T) = \left(\frac{dE_{\text{vib}}}{dT} \right)_V = 3 k_B N \left[4D \left(\frac{\theta_D}{T} \right) - \frac{3(\theta_D/T)}{e^{\theta_D/T} - 1} \right] \quad [53]$$

$$S(T) = \int_0^T \frac{C_p}{T} dT = k_B N [4D(\theta_D/T) - 3 \ln(1 - e^{-\theta_D/T})] \quad [54]$$

where

$$D(x) = \frac{3}{x^3} \int_0^x \frac{x^3 dx}{e^x - 1}, \quad x = \frac{\theta_D}{T}$$

The first term in [52] is the zero-point energy in the Debye model, the second term is the heat content. The Debye temperature is determined by the elastic properties of the solid or, more precisely, its average sound velocity $\langle v \rangle$:

$$\theta_D = \frac{\hbar}{k_B} \left(\frac{6\pi^2 N}{V} \right)^{1/3} \langle v \rangle \quad [55]$$

The mean sound velocity can be accurately calculated from the elastic constants tensor (Robie and Edwards, 1966). Usually, however, an approximate formula is used:

$$\langle v \rangle = \left(\frac{1}{v_p^3} + \frac{2}{v_s^3} \right)^{-1/3} \quad [56]$$

where v_p and v_s are the longitudinal and transverse sound velocities, respectively. Later in this chapter we shall see as to how to calculate these velocities. The advantages of the Debye model are its relative simplicity and correct low- and high-temperature limits for all thermodynamic properties. The crucial disadvantage is that it is hardly capable of giving accurate entropies for anything other than monatomic lattices. Deep theoretical analyses of this model and its critique can be found in Seitz (1949) and Kieffer (1979). In **Figure 2** we compare the phonon spectra and C_V obtained in the Debye model and in full-phonon harmonic calculations done with the same model

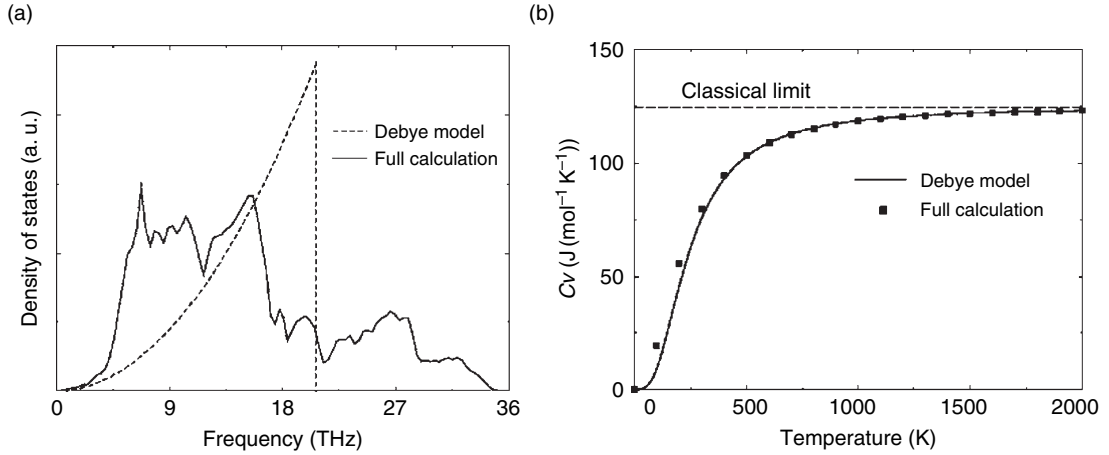


Figure 2 Phonon density of state (a) and heat capacity C_V of MgSiO₃ perovskite. Reproduced from Oganov AR, Brodholt JP, and Price GD (2000) Comparative study of quasiharmonic lattice dynamics, molecular dynamics and Debye model in application to MgSiO₃ perovskite. *Physics of the Earth and Planetary Interiors* 122: 277–288, with permission from Elsevier.

interatomic potential (see Oganov *et al.* (2000)). The phonon spectra are very different, but heat capacities are reasonably close (only below ~ 500 K, the disagreement is appreciable).

2.06.1.4.2 General harmonic potential

Let us now come back to the general harmonic case. First of all, the potential [40] describing a simple elastic spring or a diatomic molecule can be generalized to the case of three-dimensional structures. One can expand the crystal potential energy U around the equilibrium configuration in terms of displacements $u_a^i(l)$ of i th atoms in the l th unit cell along each α th coordinate (Cartesian) axis:

$$\begin{aligned}
 U = & U_0 + \sum_{l,i,\alpha} \Phi_{\alpha}^i(l) u_{\alpha}^i(l) \\
 & + \frac{1}{2!} \sum_{l < l', i < j, a, b} \Phi_{\alpha\beta}^{ij}(ll') u_{\alpha}^i(l) u_{\beta}^j(l') \\
 & + \frac{1}{3!} \sum_{l < l' < l'', j < k, \alpha, \beta, \gamma} \Phi_{\alpha\beta\gamma}^{ijk}(ll'l'') u_{\alpha}^i(l) u_{\beta}^j(l') u_{\gamma}^k(l'') \\
 & + \dots
 \end{aligned} \tag{57}$$

where

$$\begin{aligned}
 \Phi_{\alpha}^i(l) &= \frac{\partial U}{\partial u_{\alpha}^i(l)} \\
 \Phi_{\alpha\beta}^{ij}(ll') &= \frac{\partial^2 U}{\partial u_{\alpha}^i(l) \partial u_{\beta}^j(l')} \\
 \Phi_{\alpha\beta\gamma}^{ijk}(ll'l'') &= \frac{\partial^3 U}{\partial u_{\alpha}^i(l) \partial u_{\beta}^j(l') \partial u_{\gamma}^k(l'')}
 \end{aligned} \tag{58}$$

At equilibrium $\Phi_{\alpha}^i(l) = 0$, so neglecting third- and higher-order terms (called anharmonic terms), we obtain the harmonic expansion of the potential energy:

$$U = U_0 + \frac{1}{2} \sum_{l < l', i < j, a, b} \Phi_{\alpha\beta}^{ij}(ll') u_{\alpha}^i(l) u_{\beta}^j(l') \tag{59}$$

The generalized harmonic potential [59] includes noncentral forces, due to which directions of the displacement and force may differ. In spite of the complicated mathematical form of [59], it is really analogous to [40]. It also corresponds to a set of phonons, which are again noninteracting and have the same quantization as given by [41]. For each vibrational mode, the partition function is expressed as [42], and thermodynamic properties are described by [47]–[50].

The use of the harmonic approximation, neglecting third- and higher-order terms in the interatomic potential, leads to a number of fundamental errors. The phonon frequencies in this approximation do not depend on temperature or volume, and are noninteracting. This leads to a simple interpretation of experimentally observed vibrational spectra and greatly simplifies the calculation of thermodynamic properties [47]–[50], but noninteracting phonons can freely travel within the crystal, leading to an infinite thermal conductivity of the harmonic crystal. In a real crystal, thermal conductivity is, of course, finite due to phonon–phonon collisions, scattering on defects, and finite crystal size. In the harmonic approximation, the energy needed to remove an atom from the crystal is infinite – therefore,

diffusion and melting cannot be explained within this approximation. The same can be said about displacive phase transitions – even though the harmonic approximation can indicate such a transition by showing imaginary phonon frequencies, calculation of properties of the high-temperature dynamically disordered phase is out of reach of the harmonic approximation. In the harmonic approximation there is no thermal expansion, which obviously contradicts experiment. Related to this is the equality $C_V = C_P$, whereas experiment indicates $C_V < C_P$ (see [32]). In a harmonic crystal, at high temperatures C_V tends exactly to the Dulong–Petit limit of $3Nk_B$, whereas for anharmonic crystals this is not the case (see Section 2.06.1.8 for more details on anharmonicity).

The first approximation correcting many of these drawbacks, the quasiharmonic approximation, as well as methods to account for higher-order anharmonicity will be discussed later in this chapter, but now let us explore some more fundamental aspects of thermodynamics.

2.06.1.5 Quantum Effects in Thermodynamics

Quantum effects are of fundamental importance for thermodynamic properties. Insufficiency of classical mechanics is apparent in any experimental determinations of the heat capacity at low temperatures.

According to classical mechanics, every structural degree of freedom has $(k_B T)/2$ worth of kinetic energy. In a harmonic solid, there is an equal amount of potential energy, so the total vibrational energy equals $3NR$, and the heat capacity C_V is then $3NR$. In a stark contrast, experiment shows C_V going to zero as T^{-3} at low temperatures. Similarly, thermal expansion goes to zero at low temperatures – in contrast to classical theory, predicting a finite value. A very important consequence is for the entropy: if, as the classical approximation claims, $C_V = 3NR$ at all temperatures, then the entropy ($S = \int_0^T (C_V/T) dT$) is infinite.

The partition function [35] includes the relevant quantum effects, and so do harmonic expression [43]–[50] for thermodynamic functions. In the classical approximation, the partition function is

$$Z_{\text{class}} = \frac{1}{N! \lambda^{3N}} \int \int e^{-\beta[U(r) + E_{\text{kin}}(p)]} dr dp \quad [60]$$

The denominator in this definition already accounts for some quantum effects. There, one has $N!$ to account for indistinguishability of same-type particles, and λ^{3N} that takes into account the fact that quantum states are discrete and very small differences in coordinates/momenta of particles may correspond to the same quantum state. Nevertheless, this definition is classical – since it involves integration in the phase space, rather than summation over discrete quantum states and since some essentially quantum effects (such as exchange) are not present in [60].

According to the uncertainty principle, quantum particles are never at rest and there is quantum motion of atoms even at 0 K (zero-point motion). The corresponding energy, arising from quantum motion in a potential field, is called the zero-point energy, which we already encountered in harmonic expressions [43], [46], [47], and [50]. The magnitude of zero-point motion is significant – it can contribute more than 50% of the total experimentally observed atomic mean-square displacements at room temperature.

It is important that at temperatures significantly exceeding the characteristic temperatures θ of all the vibrational modes ($\theta = (\hbar\omega/k_B)$), classical expressions will be correct. This circumstance justifies the application of methods based on classical mechanics (molecular dynamics, Monte Carlo, etc.) in simulations of materials at high temperatures. At low temperatures, where quantum effects dominate, one could use the harmonic approximation (or, better, the quasiharmonic approximation – see below) or include quantum corrections to classical results.

The classical free energy can be calculated as

$$F_{\text{class}} = E_0 - k_B T \ln Z_{\text{class}} \quad [61]$$

where E_0 is the internal energy of a static crystal structure. The quantum correction to [61] per atom in the lowest order is (Landau and Lifshitz, 1980)

$$\begin{aligned} \Delta F = F - F_{\text{class}} &= \frac{\hbar^2}{24k_B^2 T^2} \left\langle \sum_i \frac{(\nabla_i U)^2}{m_i} \right\rangle \\ &= \frac{\hbar^2}{24k_B T} \left\langle \sum_i \frac{\nabla_i^2 U}{m_i} \right\rangle \end{aligned} \quad [62]$$

where ∇_i^2 is the Laplacian with respect to the coordinates of the i th atom. Higher-order (\hbar^3 and higher) corrections are needed only at temperatures below $\sim(\theta_D/2)$. Quantum corrections to other properties can be worked out by differentiating [62] (see Matsui (1989) and Figure 3).

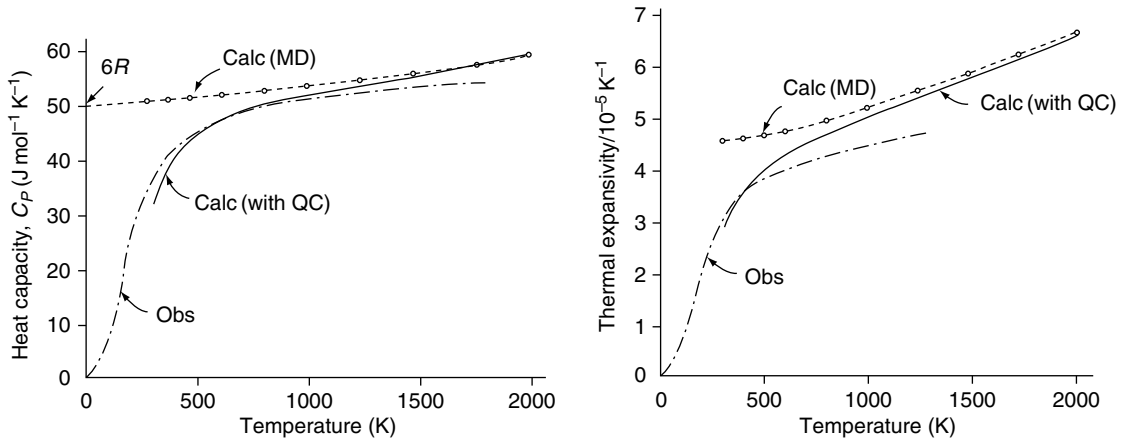


Figure 3 Heat capacity C_P and thermal expansion of MgO from classical molecular dynamics and with quantum corrections [5.3]. After Matsui M (1989) Molecular dynamics study of the structural and thermodynamic properties of MgO crystal with quantum correction. *Journal of Chemical Physics* 91: 489–494.

Other possibilities to incorporate quantum corrections into classical results can be done using (1) path integral formalism (see Allen and Tildesley, 1987), (2) phonon density of states $g(\omega)$, which can be calculated classically, and quasiharmonic formulas. Montroll (1942, 1943) has formulated a method of calculating thermodynamic properties of a solid without the knowledge of $g(\omega)$ but using moments of the frequency distribution instead.

Defining the moments as

$$\mu_{2k} = \frac{1}{3N} \int_0^\infty \omega^{2k} g(\omega) d\omega \quad [63]$$

when $T > \hbar\omega_{\max}/k_B$ one can write

$$E(T) = 3Nk_B T - 3Nk_B T \times \sum_{n=1}^\infty \frac{(-1)^n B_n}{(2n)!} \left(\frac{\hbar}{2k_B T}\right)^{2n} \mu_{2n} \quad [64]$$

$$C_V(T) = 3Nk_B - 3Nk_B \times \sum_{n=1}^\infty \frac{(-1)^n B_n (1-2n)}{(2n)!} \left(\frac{\hbar}{2k_B T}\right)^{2n} \mu_{2n} \quad [65]$$

where B_n are Bernoulli numbers. First terms in [64] and [65] are classical contributions, the second terms (sums) can be considered as quantum corrections. Taking only the first few terms, [65] takes the following form:

$$C_V(T) \approx 3Nk_B \left[1 - \left(\frac{\hbar}{k_B T}\right)^2 \frac{\mu_2}{12} + \left(\frac{\hbar}{k_B T}\right)^4 \frac{\mu_4}{240} - \left(\frac{\hbar}{k_B T}\right)^6 \frac{\mu_6}{6048} + \dots \right] \quad [66]$$

The lowest-order quantum term is, as expected, of order \hbar^2 .

2.06.1.6 Thermodynamic Perturbation Theory

It can be demonstrated (Landau and Lifshitz, 1980) that by modifying the potential energy of the system from U_0 to U_1 so that $V = U_1 - U_0$ is a small perturbation, to first order the free energy becomes

$$F_1 = F_0 + \langle V \rangle_0 \quad [67]$$

where subscript ‘0’ means that averaging is performed over the configurations of the unperturbed system. This means that the free energy of a system with the potential U_1 can be found by thermodynamic integration from (any) system U_0 , the free energy of which is known:

$$F_1 = F_0 + \int_{\lambda=0}^1 U_\lambda d\lambda \quad [68]$$

where $U_\lambda = (1-\lambda)U_0 + \lambda U_1$. The same ideas can be used to calculate the free energy profile along the chemical reaction coordinate, or generally the free energy surface – as done in metadynamics simulations (Laio and Parrinello, 2002; Iannuzzi *et al.*, 2003).

To second order, we have

$$F_1 = F_0 + \langle V \rangle_0 - \frac{1}{2k_B T} \langle (V - \bar{V})^2 \rangle_0 \quad [69]$$

where \bar{V} is the averaged perturbing potential. Note that the expressions [67] and [69] are classical, but quantum extensions are available (Landau and

Lifshitz, 1980). Thermodynamic perturbation theory plays an important role in methods to calculating free energies.

2.06.1.7 Quasiharmonic Approximation

In this approximation, it is assumed that the solid behaves like a harmonic solid at any volume, but the phonon frequencies depend on volume. It is assumed that they depend only on volume – that is, heating at constant volume does not change them.

In the quasiharmonic approximation (QHA) phonons are still independent and noninteracting. Thermodynamic functions at constant volume, as before, are given by [47]–[50], C_V still cannot exceed $3NR$. Melting, diffusion, and dynamically disordered phases are beyond the scope of this approximation, which breaks down at high temperatures. Thermal conductivity is still infinite.

However crude, this approximation heals the biggest errors of the harmonic approximation. Introducing a volume dependence of the frequencies is enough to create nonzero thermal expansion and account for $C_V < C_P$ [32]. Thermal pressure contributes to all constant-pressure thermodynamic functions (enthalpy H , Gibbs free energy G , isobaric heat capacity C_P , etc.). This is the first approximation to the thermal equation of state of solids, which can be effectively used in conjunction with realistic interatomic potentials (Parker and Price, 1989; Kantorovich, 1995; Gale, 1998) or quantum-mechanical approaches such as density-functional perturbation theory (Baroni *et al.*, 1987, 2001). For instance, using the QHA and calculating phonon frequencies using density-functional theory, Karki and co-authors calculated high-pressure thermal expansion and elastic constants of MgO (Karki *et al.*, 1999) and thermal expansion of MgSiO₃ perovskite (Karki *et al.*, 2000). Using similar methodology, Oganov and colleagues calculated a number of mineral phase diagrams – MgO, SiO₂, MgSiO₃, Al₂O₃. They found that MgO retains the NaCl-type structure at all conditions of the Earth's mantle (Oganov *et al.*, 2003) and that phase transitions of SiO₂ do not correspond to any observed seismic discontinuities in the mantle (Oganov *et al.*, 2005a). For MgSiO₃ (Oganov and Ono, 2004) and Al₂O₃ (Oganov and Ono, 2005), new high-pressure 'post-perovskite' phases with the CaIrO₃-type structure were found to be stable, and their P – T stability fields were predicted and, in the same papers, experimentally verified. Also using the QHA and

density-functional perturbation theory, Tsuchiya *et al.* (2004) studied stability of MgSiO₃ post-perovskite and confirmed previous experimental (Murakami *et al.*, 2004; Oganov and Ono, 2004) and theoretical (Oganov and Ono, 2004) findings. Oganov and Price (2005) confirmed that MgSiO₃ perovskite and post-perovskite remain stable against decomposition at all conditions of the Earth's mantle, but their decomposition into MgO and SiO₂ was predicted to occur at conditions of cores of extraterrestrial giant planets (Umemoto *et al.*, 2006).

2.06.1.8 Beyond the QHA

At temperatures roughly below one-half to two-thirds of the melting temperature, QHA is quite accurate. Only at higher temperatures do its errors become significant. All the effects beyond the QHA are known as 'intrinsic anharmonicity'. For instance, phonon–phonon interactions, displacive phase transitions, and explicit temperature dependence of the vibrational frequencies (which is experimentally measurable) are intrinsic anharmonic phenomena. Here we focus on the role of intrinsic anharmonicity in thermodynamics and equations of state of solids, rather than on aspects related to thermal conductivity and phonon–phonon interactions.

This simplest way of treating intrinsic anharmonicity takes advantage of the fact that in the high-temperature expansion of the anharmonic free energy, the lowest-order term is quadratic (Landau and Lifshitz, 1980; Zharkov and Kalinin, 1971; Gillet *et al.*, 1999). Explicit molecular dynamics simulations for MgO (Figure 4) show that third- and fourth-order terms still play some role, but overall the T^2 -term dominates. Limiting ourselves to this term, we write

$$\frac{F_{\text{anh}}(V, T)}{3Nk_B} = \frac{1}{2}aT^2 \quad [70]$$

where a is intrinsic anharmonicity parameter, usually of order 10^{-5} K^{-1} . Equation [70] assumes that intrinsic anharmonic contributions from different modes are additive. This is clearly a simplification, but it finds some justification in the arguments of Wallace (1998). Intrinsic anharmonicity normally decreases with pressure, which can be accounted for by a simple volume dependence (Zharkov and Kalinin, 1971):

$$a = a_0 \left(\frac{V}{V_0} \right)^m \quad [71]$$

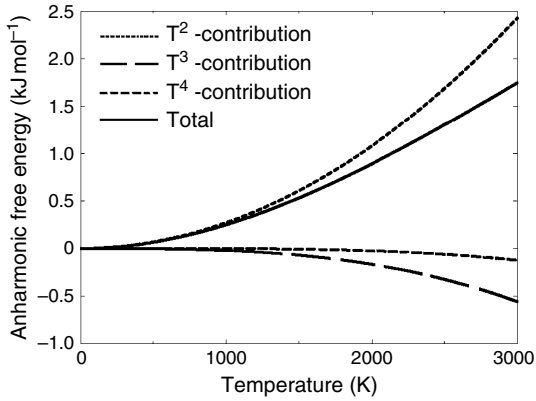


Figure 4 Intrinsic anharmonic free energy of MgO. From Oganov AR and Dorogokupets PI (2004) Intrinsic anharmonicity in thermodynamics and equations of state of solids. *Journal of Physics – Condensed Matter* 16: 1351–1360.

where a_0 is the intrinsic anharmonicity parameter at standard conditions, and $m = (d \ln a / d \ln V)$ is a constant.

One can easily find other anharmonic thermodynamic properties, such as the entropy, energy, isochoric heat capacity, thermal pressure, and bulk modulus:

$$\begin{aligned} \frac{S_{\text{anh}}}{3Nk_B} &= -aT, & \frac{E_{\text{anh}}}{3Nk_B} &= -\frac{1}{2}aT^2 \\ \frac{C_{V,\text{anh}}}{3Nk_B} &= -aT, & \frac{P_{\text{anh}}}{3Nk_B} &= -\frac{1}{2}a\frac{m}{V}T^2 \\ K_{Ta} &= P_a(1-m) \end{aligned} \quad [72]$$

This model works well at high temperatures. However, at low temperatures there are problems: linear anharmonic heat capacity [72] overwhelms the harmonic term, leading to large errors in the thermal expansion coefficient below ~ 100 K. The problem is that [70] and [72] are classical equations and completely ignore quantum vibrational effects, which determine low-temperature thermodynamics.

Wallace (1998) has shown that in the first approximation intrinsic anharmonic effects can be incorporated by using the true (i.e., temperature-dependent) vibrational frequencies ω (or characteristic temperatures $\theta = \hbar\omega/k_B$) and substituting them into the (quasi)harmonic expression for the entropy for a harmonic oscillator [45]. The result will contain both quasiharmonic and intrinsic anharmonic contributions. We follow Gillet *et al.* (1999) and define the temperature-dependent characteristic temperature as

$$\Theta_{VT} = \theta \exp(aT) \quad [73]$$

where θ is the quasiharmonic (only volume-dependent) characteristic temperature. Equation [73] thus defines the physical meaning of this parameter as the logarithmic derivative of the vibrational frequency (or characteristic temperature) with respect to volume:

$$a = \left(\frac{\partial \ln \omega_{VT}}{\partial T} \right)_V = \left(\frac{\partial \ln \Theta_{VT}}{\partial T} \right)_V \quad [74]$$

In the classical limit ($\Theta_{VT}/T \rightarrow 0$) eqns [70] and [72] are easily derived from [74].

Another approach to include quantum corrections in anharmonic properties is offered by thermodynamic perturbation theory of an anharmonic oscillator (see Oganov and Dorogokupets (2004)). Consider a general anharmonic potential

$$U_1 = \frac{1}{2}kx^2 + a_3x^3 + a_4x^4 + \dots \quad [75]$$

with $k > 0$.

As a reference system we take a harmonic oscillator

$$U_0 = \frac{1}{2}kx^2 \quad [76]$$

Using first-order thermodynamic perturbation theory [69] anharmonic free energy can be calculated as follows:

$$\begin{aligned} F_{\text{anh}} &= \langle U - U_0 \rangle_0 = \langle a_3x^3 + a_4x^4 + \dots \rangle_0 \\ &= a_4 \langle x^4 \rangle_0 + a_6 \langle x^6 \rangle_0 + a_8 \langle x^8 \rangle_0 \\ &\quad + \dots \end{aligned} \quad [77]$$

This expression is remarkable in that the moments of atomic displacements used are those of a harmonic oscillator, and can be easily calculated. Since the harmonic reference potential is symmetric, only even-order terms are retained in [77]. Truncating at the $\langle x^4 \rangle_0$ term, Oganov and Dorogokupets (2004) found

$$\frac{F_{\text{anh}}}{3n} = \frac{a}{6k_B} [\langle E \rangle^2 + 2k_B C_V T^2] \quad [78]$$

Other thermodynamic functions are easy to derive from F_{anh} by differentiation. From [78], one trivially obtains anharmonic zero-point energy:

$$\frac{E_{\text{anh}}^{\text{z.p.}}}{3n} = \frac{a}{24} k_B \theta^2 \quad [79]$$

For typical values of parameters ($a = 2 \times 10^{-5} \text{ K}^{-1}$, $\theta = 1000 \text{ K}$), this value amounts to only 0.17% of the harmonic zero-point energy. For more details on this formalism, see Oganov and Dorogokupets (2004).

Computationally, intrinsic anharmonic effects can be fully accounted for by the use of Monte Carlo or molecular dynamics simulations (Allen and Tildesley, 1987): these methods involve a full sampling of the potential hypersurface without any assumptions regarding its shape or the magnitude of atomic vibrations; these methods are also applicable to liquids and gases. Free energies of significantly anharmonic systems can be calculated using thermodynamic integration technique (e.g., Allen and Tildesley, 1987). For example, using this technique Alfè *et al.* (1999) calculated the melting curve of Fe at conditions of the Earth's core and provided first-order estimates of core temperatures (more accurate estimates were later obtained taking into account the effects of alloying elements, see Alfè *et al.* (2002)).

2.06.2 Equations of State and Elasticity

Equations of state (EOSs) (i.e., the P - V - T relationships) of Earth-forming minerals are of special interest – indeed, accurate EOSs of minerals are necessary for the interpretation of seismological observations. The importance of the elastic constants for Earth sciences springs from the fact that most of the information about the deep Earth is obtained seismologically, by measuring the velocities of seismic waves passing through the Earth. Seismic wave velocities, in turn, are related to the elastic constants of Earth-forming rocks and minerals. Acoustic anisotropy of the Earth, measurable seismologically, is related to the elastic anisotropy of Earth-forming minerals and the degree of their alignment.

2.06.2.1 Equations of State

Generally, thermodynamics gives

$$P = -\left(\frac{\partial F}{\partial V}\right)_T \quad \text{and} \quad V = \left(\frac{\partial G}{\partial P}\right)_T \quad (\text{Isothermal EOS})$$

$$T = \left(\frac{\partial H}{\partial S}\right)_P \quad \text{and} \quad S = -\left(\frac{\partial G}{\partial T}\right)_P \quad (\text{Isobaric EOS})$$

$$P = -\left(\frac{\partial E}{\partial V}\right)_S \quad \text{and} \quad V = -\left(\frac{\partial H}{\partial P}\right)_S \quad (\text{Adiabatic EOS})$$

An explicit analytical EOS can only be written for an ideal gas (where interatomic interactions are absent; in the case, there are no problems in the analytical representation of the interatomic potential, and entropy can be easily and exactly calculated using

the Sackur–Tetrode relation). For solids and liquids interatomic interactions are essential, and all existing analytical EOSs are by necessity approximate. Even worse, interactions between atoms make phase transitions possible, and EOS becomes discontinuous (i.e., nonanalytical) at phase transitions. All the approximate EOS formulations are valid only for one phase (though for a phase transition involving only small structural changes it is possible to formulate a single EOS describing two or more phases – see, e.g., Tröster *et al.* (2002)), and generally the accuracy of the EOS is best at conditions far from phase transitions.

2.06.2.1.1 Mie–Grüneisen EOS

To advance further, consider the isothermal EOS $P = -(\partial F/\partial V)_T$, taking the QHA as the starting point. Using indices i and \mathbf{k} to denote the number of the phonon branch and the wave vector \mathbf{k} , we can write a formula analogous to [50]:

$$F(T) = E_0 + \frac{1}{2} \sum_{i,\mathbf{k}} \hbar \omega_{i\mathbf{k}} + k_B T \sum_{i,\mathbf{k}} \ln \left[1 - \exp\left(-\frac{\hbar \omega_{i\mathbf{k}}}{k_B T}\right) \right] \quad [80]$$

From this, we have

$$P(V, T) = P_{\text{st}}(V) + \frac{1}{2} \sum_{i,\mathbf{k}} \hbar \frac{\gamma_{i\mathbf{k}} \omega_{i\mathbf{k}}}{V} + \sum_{i,\mathbf{k}} \frac{\gamma_{i\mathbf{k}}}{V} \frac{\hbar \omega_{i\mathbf{k}}}{\exp(\hbar \omega_{i\mathbf{k}}/k_B T) - 1} \quad [81]$$

where $P_{\text{st}}(V)$ is the static pressure, and the mode Grüneisen parameter $\gamma_{i\mathbf{k}}$ is defined as

$$\gamma_{i\mathbf{k}} = -\left(\frac{\partial \ln \omega}{\partial \ln V}\right)_T \quad [82]$$

In the QHA, the Grüneisen parameter is temperature independent.

At high temperatures or when all $\gamma_{i\mathbf{k}}$ are equal, [81] can be simplified:

$$P(V, T) = P_{\text{st}}(V) + \gamma \frac{E_{\text{vib}}(V, T)}{V} \quad [83]$$

where

$$\gamma = \langle \gamma_{i\mathbf{k}} \rangle \quad [84]$$

Equation [83] is the famous Mie–Grüneisen thermal EOS. It should be noted that in the classical approximation, which is put in the basis of the standard molecular dynamics and Monte Carlo simulations, the thermodynamic Grüneisen parameter

will always be close to $\langle \gamma_{nk} \rangle$ (Welch *et al.*, 1978), but it will also include a temperature-dependent correction due to intrinsic anharmonic effects.

As shown by Holzapfel (2001), the three common definitions of the Grüneisen parameter (via the thermal pressure, thermal expansion, and volume derivatives of the phonon frequencies)

$$\gamma_P(V, T) = \frac{P_{\text{vib}}}{E_{\text{vib}}} V \quad [85a]$$

$$\gamma_\alpha(V, T) = \alpha \frac{K_T V}{C_V} \quad [85b]$$

$$\gamma_{\text{qh}}(V) = \left\langle \frac{-d \ln \omega_i}{d \ln V} \right\rangle \quad [85c]$$

are all identical for a classical quasiharmonic solid, and all different for a system with intrinsic anharmonicity. Very roughly, $\gamma_P(V, T)$ is halfway between $\gamma_{\text{qh}}(V)$ and $\gamma_\alpha(V, T)$, that is, anharmonic effects are much pronounced in thermal expansion than in thermal pressure. We stress that care must be taken as to which definition of the Grüneisen parameter is used when analyzing experimental and theoretical results. **Figure 5** shows the different definitions of the Grüneisen parameter and that the differences are small at low temperatures, but significantly increase with temperature; also shown is the volume dependence of the parameter q :

$$q = \left(\frac{\partial \ln \gamma}{\partial \ln V} \right)_T \quad [86]$$

Often, the volume dependence of γ is described by a power law:

$$\gamma(V) = \gamma_0 \left(\frac{V}{V_0} \right)^q \quad [87]$$

where parameter q is usually assumed to be constant. However, this form becomes poor at high compression. A much better function was proposed by Al'tshuler *et al.* (1987) (see also Vorobev (1996)):

$$\gamma = \gamma_\infty + (\gamma_0 - \gamma_\infty) \left(\frac{V}{V_0} \right)^\beta \quad [88]$$

where γ_0 and γ_∞ are Grüneisen parameters at $V = V_0$ and at infinite compression ($V = 0$), respectively.

2.06.2.1.2 Analytical static EOS

Good discussions of this issue can be found in many sources, including Holzapfel (1996, 2001), Sutton (1993), Hama and Suito (1996), Cohen *et al.* (2000), Poirier (2000), and Vinet *et al.* (1986, 1989). Over the decades, many different EOS forms have been generated, but here we discuss only the ones that are most interesting from the theoretical and practical points of view.

The simplest approach is based on elasticity theory. Assuming that the bulk modulus K varies linearly with pressure and denoting $K'_0 = (\partial K / \partial P)_{P=0}$, we obtain the Murnaghan EOS:

$$P = \frac{K_0}{K'_0} \left[\left(\frac{V}{V_0} \right)^{-K'_0} - 1 \right] \quad [89]$$

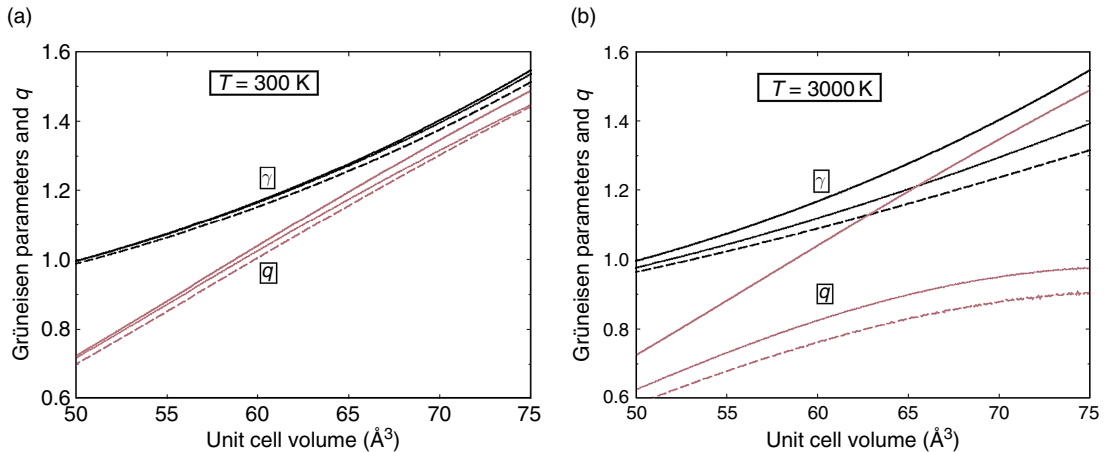


Figure 5 Grüneisen parameters and q parameters of MgO as a function of volume. (a) At 300 K, (b) at 3000 K. Solid lines indicate quasiharmonic results, dotted lines (middle) indicate γ_P , dashed lines indicate γ_α . From Oganov AR and Dorogokupets PI (2003) All-electron and pseudopotential study of MgO: Equation of state, anharmonicity, and stability. *Physical Review B* 67 (uppermost for γ and q) (art. 224110).

This simple EOS works reasonably well only in a very limited compression range. A better approach (in terms of the accuracy relative to the number of parameters of the mathematical formulation) is provided by the effective potential methods, where an approximate model for the energy as a function of $x = V/V_0$, or some other measure of strain, is used.

For example, starting from a polynomial

$$E = E_0 + af^2 + bf^3 + cf^4 + \dots \quad [90]$$

in terms of the Eulerian strain f_E : $f_E = (1/2)[x^{-2/3} - 1]$, one arrives at the family of Birch–Murnaghan EOSs. (It is advantageous to use the Eulerian finite strain rather than the Lagrangian strain $f_L = (1/2)[1 - x^{2/3}]$, because the Eulerian strain leads to a better description of the correct $E(V)$ dependence with fewer terms in the expansion [90]. At infinite pressure, Eulerian strain is infinite, whereas Lagrangian strain remains finite and will require an infinite-order expansion. However, for infinitesimal strains both definitions become equivalent.) The often used third-order Birch–Murnaghan EOS is

$$P = \frac{3}{2}K_0 [x^{-7/3} - x^{-5/3}] \left\{ 1 + \xi [x^{-2/3} - 1] \right\} \quad [91]$$

$$E = E_0 + \frac{3}{2}K_0V_0 \left[\frac{3}{2}(\xi - 1)x^{-2/3} + \frac{3}{4}(1 - 2\xi)x^{-4/3} + \frac{1}{2}\xi x^{-6/3} - \frac{2\xi - 3}{4} \right] \quad [92]$$

where $\xi = (3/4)(K'_0 - 4)$.

It is possible to derive systematically higher-order BM EOSs, but this appears to be of little use since the number of parameters involved becomes too large; only the fourth-order BM EOS

$$P = 3K_0f_E(1 + 2f_E)^{5/2} \left\{ 1 + \frac{3}{2}(K'_0 - 4)f_E + \frac{3}{2} \left[K_0K''_0 + (K'_0 - 4)(K'_0 - 3) + \frac{35}{9} \right] f_E^2 \right\} \quad [93]$$

is sometimes used when ultrahigh pressures are studied.

The Vinet EOS (Vinet *et al.*, 1986, 1989) is sometimes considered as one of the most impressive recent achievements in solid-state physics (Sutton, 1993). In fact, this is a whole family of EOSs of different orders. The most remarkable feature is its very fast convergence with respect to the order of EOS – one seldom needs to use beyond the third-order Vinet EOS.

This EOS is based on a universal scaled binding energy curve

$$E = E_0(1 + a) \exp(-a) \quad [94]$$

where E_0 is the bond energy at equilibrium, $a = (R - R_0)/l$, $l = \sqrt{E_0/(\partial^2 E/\partial R^2)}$ being a scaling length roughly measuring the width of the potential well, and R the Wigner–Seitz radius (the average radius of a sphere in the solid containing one atom). The potential [94] was invented and first used by Rydberg (1932) for fitting potential curves of molecules and obtaining their anharmonic coefficients; it turned out (Vinet *et al.*, 1986) that it describes very accurately systems with different types of chemical bonding in solids, molecules, adsorbates, etc.

The third-order Vinet EOS is (Vinet *et al.*, 1989; Hama and Suito, 1996)

$$P = 3K_0 \frac{1 - x^{1/3}}{x^{2/3}} \exp[\eta(1 - x^{1/3})] \quad [95]$$

$$E(V) = E(V_0) + \frac{9K_0V_0}{\eta^2} \left\{ 1 - [1 - \eta(1 - x^{1/3})] \times \exp[\eta(1 - x^{1/3})] \right\} \quad [96]$$

where $\eta = (3/2)(K'_0 - 1)$. The resulting expression for the bulk modulus is

$$K = \frac{K_0}{x^{2/3}} [1 + (1 + \eta x^{1/3})(1 - x^{1/3})] \exp[\eta(1 - x^{1/3})] \quad [97]$$

From this one has (Vinet *et al.*, 1989)

$$K''_0 = -\frac{1}{K_0} \left[\left(\frac{K'_0}{2} \right)^2 + \left(\frac{K'_0}{2} \right) - \frac{19}{36} \right] \quad [98]$$

The Vinet EOS proved to be very accurate for fitting EOS of solid hydrogen (Loubeyre *et al.*, 1996; Cohen *et al.*, 2000) throughout the whole experimentally studied pressure range 0–120 GPa, roughly to the eightfold compression.

In very rare cases a higher-order Vinet EOS may be needed; such higher-order versions of the Vinet EOS already exist (Vinet *et al.*, 1989):

$$P = \frac{3K_0}{x^{2/3}} (1 - x^{1/3}) \exp[\eta(1 - x^{1/3}) + \beta(1 - x^{1/3})^2 + \gamma(1 - x^{1/3})^3 + \dots] \quad [99]$$

and the fourth-order Vinet EOS, where $\beta = (1/24)(36K_0K''_0 + 9K_0'^2 + 18K'_0 - 19)$ and $\gamma = 0$, has been successfully applied to solid H₂ at extreme compressions (Cohen *et al.*, 2000) and has led to significant improvements of the description of experimental PV -data.

In the limit of extreme compressions ($x \rightarrow 0$) the Vinet EOS fails to reproduce the correct free-electron limit and gives a finite (rather than positive infinite) energy equal to $(9K_0V_0/\eta^2)[1 - (1-\eta)\exp(\eta)]$ (we do not consider here nuclear forces, which become important at densities $\sim 10^{15} \text{ g cm}^{-3}$ ($P \sim 10^{20} \text{ GPa}$) corresponding to $x < 10^{-12}$ (Holzapfel, 2001)). EOSs, manifesting the correct Thomas–Fermi behavior at extreme compressions, have been developed and discussed in detail by Holzapfel (1996, 2001) and Hama and Suito (1996).

Holzapfel (1996, 2001) has modified the Vinet EOS so as to make it satisfy the electron-gas limit at extreme compressions. His APL EOS (also a family of L th-order EOSs) is as follows (Holzapfel, 2001):

$$P = \frac{3K_0}{x^{-5/3}}(1-x^{1/3})\exp[c_0(1-x^{1/3})] \times \left\{ 1 + x^{1/3} \sum_{k=2}^L c_k(1-x^{1/3})^{k-1} \right\} \quad [100]$$

where $c_0 = -\ln(3K_0/P_{FG0})$, $P_{FG0} = a_{FG}(Z/V_0)^{5/3}$, $a_{FG} = 0.02337 \text{ GPa \AA}^5$, and Z the total number of electrons per volume V_0 .

This EOS correctly predicts that at infinite compression $K'_\infty = 5/3$ (while at $x=1$ $K'_0 = 3 + (3/2)(c_0 + c_2)$), but becomes very similar to the Vinet EOS at moderate compressions. The mathematical similarity between [99] and [100] is obvious, and it is easy to generalize these EOSs into one family. For a third-order generalized Vinet–Holzapfel EOS, one has (Kunc *et al.*, 2003)

$$P = \frac{3K_0}{x^{n/3}}(1-x^{1/3})\exp[\eta(1-x^{1/3})] \quad [101]$$

where $\eta = (3K'_0/2) + (1/2) - n$. The Vinet EOS is recovered when $n=2$, and the Holzapfel EOS is obtained when $n=5$. Kunc *et al.* (2003) found that theoretical EOS of diamond is best represented by the EOS [101] with an intermediate value $n = 7/2$. In this case, the energy can be expressed analytically:

$$E(V) = E(V_0) + 9K_0V_0[f(V) - f(V_0)] \frac{\exp(\eta)}{\sqrt{\eta}} \quad [102]$$

where

$$f(V) = \sqrt{\pi}(2\eta + 1)\text{erf}(\sqrt{\eta}x^{2/3}) + \frac{(2\sqrt{\eta}\exp(-\eta x^{1/3}))}{x^{2/3}}$$

However, it remains to be seen how accurate [102] is for other materials.

2.06.2.1.3 Anharmonicity in static EOS

Since both K' and γ come from anharmonic interactions, an intriguing possibility arises to establish a general relation between these parameters. This possibility has been widely discussed since 1939, when J. Slater suggested the first solution of the problem:

$$\gamma_s = \frac{1}{2}K' - \frac{1}{6} \quad [103]$$

Later approaches resulted in very similar equations, the difference being in the value of the constant subtracted from $(1/2)K'$: 1/2, 5/6, or 0.95. If any of the relations of the type [103] were accurate, it would greatly simplify the construction of thermal EOS. Although some linear correlation between γ and K' does exist, the correlation is too poor to be useful (Wallace, 1998; Vočadlo *et al.*, 2000).

2.06.2.1.4 EOS, internal strain, and phase transitions

All the EOSs discussed in the previous section implicitly assumed that crystal structures compress uniformly, and there is no relaxation of the unit cell shape or of the atomic positions. For some solids (e.g., MgO) this is definitely true. For most crystals and all glasses, however, this is an approximation, sometimes crude. Classical EOSs are less successful for crystals with internal degrees of freedom and perform particularly poorly in the vicinity of phase transitions. In the simplest harmonic model, Oganov (2002) obtained the following formula:

$$P(V) = P_{\text{unrelaxed}}(V) + \sum_i m_i^2(V - V_0) \quad [104]$$

with parameters m_i . $P_{\text{unrelaxed}}$ is well described by the conventional EOSs, for example, Vinet EOS, whereas the total EOS is not necessarily so (see line 2 in **Figure 6**). The bulk modulus is always lowered by the relaxation effects, in the simplest approximation [104]:

$$K(V) = K_{\text{unrelaxed}}(V) - \sum_i m_i^2V \quad [105]$$

which implies the tendency of K' to be higher than the corresponding unrelaxed value:

$$K'(V) = K'_{\text{unrelaxed}}(V) + \sum_i m_i^2 \frac{V}{K} \quad [106]$$

This simple model explains qualitatively correctly the real effects of internal strain. Complex structures are usually relatively ‘soft’ and usually have large K'_0

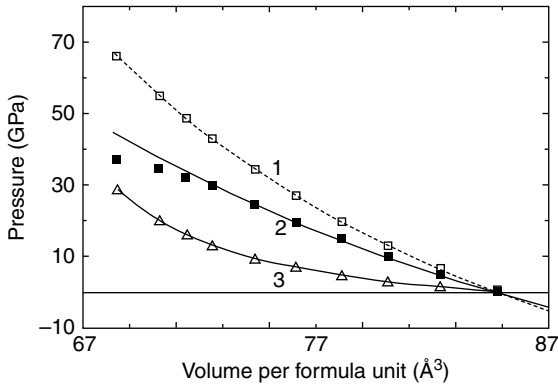


Figure 6 Effects of internal strains on equation of state. At the highest pressures shown, the structure is on the verge of an isosymmetric phase transition. 1, unrelaxed EOS; 2, correct EOS including relaxation; 3, the difference caused by relaxation. Note that in the pretransition region the full EOS is poorly fit, while the unrelaxed EOS is very well represented by analytical EOSs (in this case BM3).

(often significantly exceeding ‘normal’ $K'_0 = 4$), in agreement with the prediction [106]. For example, quartz SiO_2 , although consisting of extremely rigid SiO_2 tetrahedra, has a very low bulk modulus $K_0 = 37.12$ GPa and high $K'_0 = 5.99$ (Angel *et al.*, 1997): its structure is very flexible due to relaxation of the internal degrees of freedom. Perhaps, the highest known $K'_0 = 13$ was found in amphibole grunerite (Zhang *et al.*, 1992) with a very complicated structure having many degrees of freedom.

As an illustration, consider two series of *ab initio* calculations on sillimanite, Al_2SiO_5 (based on results from Oganov *et al.* (2001b)). In one series all structural parameters were optimized, while in the other series the zero-pressure structure was compressed homogeneously (i.e., without any relaxation). Results are shown in **Figure 6**, where a very large relaxation effect can be seen.

It is well known that internal strains always soften the elastic constants (e.g., Catti, 1989). In extreme cases, the softening can be complete, leading to a phase transition. In such cases, the simplified model [104] is not sufficient. To study EOS in the vicinity of the phase transition, one needs to go beyond the harmonic approximation built in this model. This can be done using the Landau expansion of the internal energy in powers of Q including the full elastic constants tensor and allowed couplings of the order parameter and lattice strains (see, e.g., Tröster *et al.* (2002)).

2.06.2.2 Elastic Constants

A number of excellent books and reviews exist, especially, Nye (1998), Sirotnin and Shaskolskaya (1975), Wallace (1998), Alexandrov and Prodaivoda (1993), Born and Huang (1954), Belikov *et al.* (1970), Barron and Klein (1965), and Fedorov (1968). Elastic constants characterize the ability of a material to deform under small stresses. They can be described by a fourth-rank tensor C_{ijkl} , relating the second-rank stress tensor σ_{ij} to the (also second-rank) strain tensor e_{kl} via the generalized Hooke’s law:

$$\sigma_{ij} = C_{ijkl}e_{kl} \quad [107]$$

where multiplication follows the rules of tensor multiplication (see Nye, 1998). Equation [107] can be simplified using the Voigt notation (Nye, 1998), which represents the fourth-rank tensor C_{ijkl} by a symmetric 6×6 matrix C_{ij} . In these notations, indices ‘11’, ‘22’, ‘33’, ‘12’, ‘13’, ‘23’ are represented by only one symbol – 1, 2, 3, 6, 5, and 4, respectively. So we write instead of [107]

$$\sigma_i = C_{ij}e_j \quad [108]$$

Note that infinitesimal strains are being used; in this limit, all definitions of strain (e.g., Eulerian, Lagrangian, Hencky, etc.) become equivalent. Under a small strain, each lattice vector a_{ij}' of the strained crystal is obtained from the old lattice vector a_{ij}^0 and the strain tensor e_{ij} using the relation

$$a_{ij}' = (\delta_{ij} + e_{ij})a_{ij}^0 \quad [109]$$

In the original tensor notation and in the Voigt notation (Nye, 1998), the $(\delta_{ij} + e_{ij})$ matrix is represented as follows:

$$\begin{bmatrix} 1 + e_{11} & e_{12} & e_{13} \\ e_{12} & 1 + e_{22} & e_{23} \\ e_{13} & e_{23} & 1 + e_{33} \end{bmatrix} = \begin{bmatrix} 1 + e_1 & e_6/2 & e_5/2 \\ e_6/2 & 1 + e_2 & e_4/2 \\ e_5/2 & e_4/2 & 1 + e_3 \end{bmatrix} \quad [110]$$

Voigt notation is sufficient in most situations; only in rare situations such as a general transformation of the coordinate system, the full fourth-rank tensor representation must be used to derive the transformed elastic constants.

The number of components of a fourth-rank tensor is 81; the Voigt notation reduces this to 36. The thermodynamic equality $C_{ij} = C_{ji}$ makes the 6×6

matrix of elastic constants symmetric, reducing the number of independent constants to the well-known maximum number of 21, possessed by triclinic crystals. Crystal symmetry results in further reductions of this number: 13 for monoclinic, 9 for orthorhombic, 6 or 7 (depending on the point group symmetry) for trigonal and tetragonal, 5 for hexagonal, and 3 for cubic crystals; for isotropic (amorphous) solids there are only two independent elastic constants.

One can define the inverse tensor S_{ijkl} (or, in the Voigt notation, S_{ij}), often called the elastic compliance tensor:

$$\{S_{ijkl}\} = \{C_{ijkl}\}^{-1} \quad \text{or} \quad \{S_{ij}\} = \{C_{ij}\}^{-1} \quad [111]$$

(Note that in Voigt notation $C_{ijkl} = C_{mnop}$ but $S_{ijkl} = S_{mnop}$ only when m and $n = 1, 2$, or 3 ; when either m or $n = 4, 5$, or 6 : $2S_{ijkl} = S_{mnop}$; when both m and $n = 4, 5$, or 6 : $4S_{ijkl} = S_{mnop}$ (Nye, 1998).) The S_{ij} tensor can be defined via the generalized Hooke's law in its equivalent formulation:

$$e_i = S_{ij}\sigma_j \quad [112]$$

Linear compressibilities can be easily derived from the S_{ij} tensor. Full expressions for an arbitrary direction can be found in Nye (1998); along the coordinate axes, the linear compressibilities are

$$\begin{aligned} \beta_x &= -\frac{1}{l_x} \left(\frac{\partial l_x}{\partial P} \right)_T = \sum_{j=1}^3 S_{1j} = S_{11} + S_{12} + S_{13} \\ \beta_y &= -\frac{1}{l_y} \left(\frac{\partial l_y}{\partial P} \right)_T = \sum_{j=1}^3 S_{2j} = S_{12} + S_{22} + S_{23} \\ \beta_z &= -\frac{1}{l_z} \left(\frac{\partial l_z}{\partial P} \right)_T = \sum_{j=1}^3 S_{3j} = S_{13} + S_{23} + S_{33} \end{aligned} \quad [113]$$

where l_x, l_y, l_z are linear dimensions along the axes of the coordinate system. (These axes may not coincide with the lattice vectors for nonorthogonal crystal systems. Coordinate systems used in crystal physics are always orthogonal.) For the bulk compressibility, we have

$$\begin{aligned} \beta &= -\frac{1}{V} \left(\frac{\partial V}{\partial P} \right)_T = \beta_x + \beta_y + \beta_z = \sum_{i=1}^3 \sum_{j=1}^3 S_{ij} \\ &= S_{11} + S_{22} + S_{33} + 2(S_{12} + S_{13} + S_{23}) \end{aligned} \quad [114]$$

The values of the elastic constants depend on the orientation of the coordinate system. There are two particularly important invariants of the elastic constants tensor – bulk modulus K and shear modulus G ,

obtained by special averaging of the individual elastic constants. There are several different schemes of such averaging. Reuss averaging is based on the assumption of a homogeneous stress throughout the crystal, leading to the Reuss bulk modulus:

$$K_R = \frac{1}{S_{11} + S_{22} + S_{33} + 2(S_{12} + S_{13} + S_{23})} = \frac{1}{\beta} \quad [115]$$

and shear modulus:

$$G_R = \frac{15}{4(S_{11} + S_{22} + S_{33}) - 4(S_{12} + S_{13} + S_{23}) + 3(S_{44} + S_{55} + S_{66})} \quad [116]$$

It is important to realize that it is the Reuss bulk modulus, explicitly related to compressibility, that is used in constructing EOSs and appears in all thermodynamic equations involving the bulk modulus.

Another popular scheme of averaging is due to Voigt. It is based on the assumption of a spatially homogeneous strain, and leads to the following expressions for the Voigt bulk and shear moduli:

$$\begin{aligned} K_V &= \frac{C_{11} + C_{22} + C_{33} + 2(C_{12} + C_{13} + C_{23})}{9} \\ G_V &= \frac{C_{11} + C_{22} + C_{33} - (C_{12} + C_{13} + C_{23}) + 3(C_{44} + C_{55} + C_{66})}{15} \end{aligned} \quad [117]$$

For an isotropic polycrystalline aggregate the Voigt moduli give upper and the Reuss moduli lower bounds for the corresponding moduli. More accurate estimates can be obtained from Voigt–Reuss–Hill averages:

$$K_{VRH} = \frac{K_V + K_R}{2}, \quad G_{VRH} = \frac{G_V + G_R}{2} \quad [119]$$

The most accurate results (and tighter bounds) are given by the Hashin–Shtrikman variational scheme, which is much more complicated, but leads to results similar to the Voigt–Reuss–Hill scheme (see Watt *et al.* (1976) for more details).

There are two groups of experimental methods for measuring the elastic constants: (1) static and low-frequency methods (based on determination of stress–strain relations for static stresses) and (2) high-frequency or dynamic methods (e.g., ultrasonic methods and Brillouin spectroscopy). High-frequency methods generally enable much higher accuracy. Static measurements yield isothermal elastic constants (the timescale of the experiment allows thermal equilibrium to be attained within the sample); high-frequency measurements give adiabatic

constants (Belikov *et al.*, 1970). The difference, which is entirely due to anharmonic effects (see below), vanishes at 0 K. Adiabatic C_{ij} are larger, usually by a few percent. The following thermodynamic equation gives the difference in terms of thermal pressure tensor b_{ij} (Wallace, 1998):

$$C_{ijkl}^S = C_{ijkl}^T + \frac{TV}{C_V} b_{ij} b_{kl} \quad [120]$$

where $b_{ij} = (\partial\sigma_{ij}/\partial T)_V$ is related to the thermal expansion tensor. Equation [120] implies, for the bulk moduli, the already-mentioned formula [33]:

$$K_S = K_T(1 + \alpha\gamma T) = K_T \left(1 + \frac{\alpha^2 K_T V}{C_V}\right)$$

where α and γ are the thermal expansion and Grüneisen parameter, respectively. Adiabatic and isothermal shear moduli are strictly equal for cubic crystals and usually practically indistinguishable for crystals of other symmetries.

Acoustic wave velocities measured in seismological experiments and ultrasonic determinations of elastic constants are related to the adiabatic elastic constants. Isothermal constants, on the other hand, are related to the compressibility and EOS.

The general equation for the calculation of velocities of acoustic waves with an arbitrary propagation direction, the Christoffel equation (Sirotnin and Shaskolskaya, 1975), is

$$C_{ijkl}^S \mathbf{m}_j \mathbf{m}_k p_l = \rho v^2 p_i \quad [121]$$

where ρ is the polarization vector of the wave (of unit length), \mathbf{m} the unit vector parallel to the wave vector, and ρ the density of the crystal. It can also be represented in the form of a secular equation:

$$\det||C_{ijkl}^S \mathbf{m}_j \mathbf{m}_k - \rho v^2 \delta_{il}|| = 0 \quad [122]$$

This equation has three solutions, one of which corresponds to a longitudinal, and the other two to transverse waves (see, e.g., **Figure 7**). For example, one can obtain the following velocities for a cubic crystal along high-symmetry directions:

$$\begin{aligned} (a) \quad \mathbf{m} = [100]: \quad v_1 &= \sqrt{\frac{C_{11}}{\rho}} \quad (\mathbf{p} = [100]) \\ v_2 &= \sqrt{\frac{C_{44}}{\rho}} \quad (\mathbf{p} = [010]) \\ v_3 &= \sqrt{\frac{C_{44}}{\rho}} \quad (\mathbf{p} = [001]) \end{aligned}$$

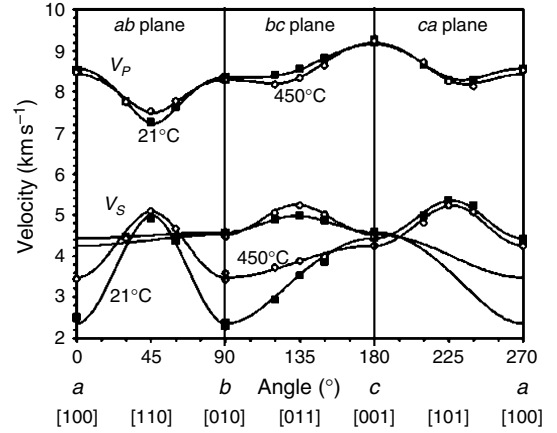


Figure 7 Acoustic velocities as a function of the propagation direction in lawsonite $\text{CaAl}_2(\text{Si}_2\text{O}_7)(\text{OH})_2 \cdot \text{H}_2\text{O}$. Solid squares, at 21°C; open circles, 450°C. Reproduced from Schilling FR, Sinogeikin SV, and Bass JD (2003) Single-crystal elastic properties of lawsonite and their variation with temperature. *Physics of the Earth and Planetary Interiors* 136: 107–118, with permission from Elsevier.

$$\begin{aligned} (b) \quad \mathbf{m} = [110]: \quad v_1 &= \sqrt{\frac{C_{11} + C_{12} + 2C_{44}}{2\rho}} \quad (\mathbf{p} = [110]) \\ v_2 &= \sqrt{\frac{C_{44}}{\rho}} \quad (\mathbf{p} = [001]) \\ v_3 &= \sqrt{\frac{C_{11} - C_{12}}{\rho}} \quad (\mathbf{p} = [1\bar{1}0]) \end{aligned}$$

The average velocities are given by famous equations (Belikov *et al.*, 1970)

$$v_p = \sqrt{\frac{3K + 4G}{3\rho}} \quad [123]$$

and

$$v_s = \sqrt{\frac{G}{\rho}} \quad [124]$$

where the adiabatic Voigt–Reuss–Hill (or Hashin–Shtrikman) values are used for the bulk and shear moduli.

At constant P, T , the elastic constants describing stress–strain relations [107] are given by

$$C_{ijkl}^T = \frac{1}{V} \left(\frac{\partial^2 G}{\partial e_{ij} \partial e_{kl}} \right)_T \quad [125]$$

while at constant P, S , they are

$$C_{ijkl}^S = \frac{1}{V} \left(\frac{\partial^2 H}{\partial e_{ij} \partial e_{kl}} \right)_S \quad [126]$$

Now let us derive from [125] an expression for the elastic constants in terms of the second derivatives of the internal energy; in this derivation, we follow Ackland and Reed (2003). The unit cell of a crystal can be represented by a matrix $\vec{V} = (\mathbf{a}_1, \mathbf{a}_2, \mathbf{a}_3)$, and the volume of the equilibrium unit cell is then $V_0 = \det \vec{V}$. Using [109], for the volume V of a strained cell we obtain

$$\begin{aligned} \frac{V}{V_0} = \frac{\det \vec{V}}{\det \vec{V}_0} = & 1 + e_1 + e_2 + e_3 + e_1 e_2 + e_2 e_3 \\ & + e_1 e_3 - \frac{e_4^2}{4} - \frac{e_5^2}{4} - \frac{e_6^2}{4} \\ & + e_1 e_2 e_3 - \frac{e_1 e_4^2}{4} - \frac{e_2 e_5^2}{4} \\ & - \frac{e_3 e_6^2}{4} + \frac{e_4 e_5 e_6}{4} \end{aligned} \quad [127]$$

Then one has in the standard tensor notation

$$\frac{\Delta V}{V_0} = e_{ii} + \frac{1}{4} (2\delta_{ij}\delta_{kl} - \delta_{ik}\delta_{jl} - \delta_{il}\delta_{jk}) e_{ij} e_{kl} + O(e^3) \quad [128]$$

Then, the change of the Gibbs free energy associated with strain is, to the second order,

$$\Delta G = \Delta F + P e_{ii} + \frac{PV}{4} (2\delta_{ij}\delta_{kl} - \delta_{ik}\delta_{jl} - \delta_{il}\delta_{jk}) e_{ij} e_{kl} \quad [129]$$

From this one has

$$C_{ijkl}^T = \frac{1}{V} \left(\frac{\partial^2 F}{\partial e_{ij} \partial e_{kl}} \right)_T + \frac{P}{2} (2\delta_{ij}\delta_{kl} - \delta_{ik}\delta_{jl} - \delta_{il}\delta_{jk}) \quad [130a]$$

and, by analogy,

$$C_{ijkl}^S = \frac{1}{V} \left(\frac{\partial^2 F}{\partial e_{ij} \partial e_{kl}} \right)_S + \frac{P}{2} (2\delta_{ij}\delta_{kl} - \delta_{ik}\delta_{jl} - \delta_{il}\delta_{jk}) \quad [130b]$$

It is well known (Barron and Klein, 1965; Wallace, 1998) that under nonzero stresses there can be several different definitions of elastic constants. The constants C_{ijkl}^T and C_{ijkl}^S defined by eqns [130a] and [130b] are those appearing in stress–strain relations and in the conditions of mechanical stability of crystals (see below), whereas the long-wavelength limit of lattice dynamics is controlled by

$$\frac{1}{V} \left(\frac{\partial^2 E}{\partial e_{ij} \partial e_{kl}} \right)_S$$

These two definitions (via stress–strain relations and from long-wavelength lattice dynamics) become identical at zero pressure.

Calculating the second derivatives with respect to the finite Lagrangian strains η_{ij} , different equations

are obtained (Wallace, 1998) for the case of hydrostatic pressure:

$$C_{ijkl}^S = \frac{1}{V} \left(\frac{\partial^2 E}{\partial \eta_{ij} \partial \eta_{kl}} \right)_S + P (\delta_{ij}\delta_{kl} - \delta_{il}\delta_{jk} - \delta_{jl}\delta_{ik}) \quad [131a]$$

$$C_{ijkl}^T = \frac{1}{V} \left(\frac{\partial^2 F}{\partial \eta_{ij} \partial \eta_{kl}} \right)_T + P (\delta_{ij}\delta_{kl} - \delta_{il}\delta_{jk} - \delta_{jl}\delta_{ik}) \quad [131b]$$

For a general stress the analogous equations are

$$\begin{aligned} C_{ijkl}^S = \frac{1}{V} \left(\frac{\partial^2 E}{\partial \eta_{ij} \partial \eta_{kl}} \right)_S \\ - \frac{1}{2} (2\sigma_{ij}\delta_{kl} - \sigma_{ik}\delta_{jl} - \sigma_{il}\delta_{jk} - \sigma_{jl}\delta_{ik} - \sigma_{jk}\delta_{il}) \end{aligned} \quad [132a]$$

$$\begin{aligned} C_{ijkl}^T = \frac{1}{V} \left(\frac{\partial^2 F}{\partial \eta_{ij} \partial \eta_{kl}} \right)_T \\ - \frac{1}{2} (2\sigma_{ij}\delta_{kl} - \sigma_{ik}\delta_{jl} - \sigma_{il}\delta_{jk} - \sigma_{jl}\delta_{ik} - \sigma_{jk}\delta_{il}) \end{aligned} \quad [132b]$$

Cauchy relations, originally derived with the definition via the energy density, can be elegantly formulated in this definition as well (see below). Note, however, that the elastic constants C_{ijkl} , defined from stress–strain relations, have the full Voigt symmetry only at hydrostatic pressure. It is essential to distinguish between different definitions of elastic constants under pressure.

2.06.2.2.1 Cauchy relations

For crystals where all atoms occupy centrosymmetric positions, and where all interatomic interactions are central and pairwise (i.e., depend only on the distances between atoms, and not on angles), in the static limit Cauchy relations (Born and Huang, 1954; but take into account eqns [130a] and [130b] hold:

$$\begin{aligned} C_{23} - C_{44} = 2P; \quad C_{31} - C_{55} = 2P; \quad C_{12} - C_{66} = 2P \\ C_{14} - C_{56} = 0; \quad C_{25} - C_{64} = 0; \quad C_{36} - C_{45} = 0 \end{aligned} \quad [133]$$

These relations would reduce the maximum number of independent elastic constants to 15; however, they never hold exactly because there are always noncentral and many-body contributions to crystal energy. Violations of the Cauchy relations can serve as a useful indicator of the importance of such interactions. While for many alkali halides Cauchy relations hold reasonably well, for alkali earth oxides (e.g., MgO) they are grossly violated. This is because the free O^{2-} ion is unstable and can exist only in the crystalline environment due to the stabilizing Madelung potential created by all atoms in the crystal; the charge density around O^{2-} is thus very susceptible to the changes of structure,

including strains. Consequently, interactions of the O^{2-} ion with any other ion depend on the volume of the crystal and location of all other ions; this is a major source of many-body effects in ionic solids. This point of view is strongly supported by the success of potential induced breathing (PIB; see Bukowinski (1994) and references therein) and similar models in reproducing the observed Cauchy violations. In these models, the size of an O^{2-} ion (more precisely, the radius of the Watson sphere stabilizing the O^{2-}) depends on the classical electrostatic potential induced by other ions.

2.06.2.2.2 Mechanical stability

One of the most common types of instabilities occurring in crystals is the so-called mechanical instability, when some of the elastic constants (or their special combinations) become zero or negative. The condition of mechanical stability is the positive definiteness of the elastic constants matrix:

$$\begin{array}{cccccc}
 C_{11} & C_{12} & C_{13} & C_{14} & C_{15} & C_{16} \\
 \hline
 C_{21} & C_{22} & C_{23} & C_{24} & C_{25} & C_{26} \\
 \hline
 C_{31} & C_{32} & C_{33} & C_{34} & C_{35} & C_{36} \\
 \hline
 C_{41} & C_{42} & C_{43} & C_{44} & C_{45} & C_{46} \\
 \hline
 C_{51} & C_{52} & C_{53} & C_{54} & C_{55} & C_{56} \\
 \hline
 C_{61} & C_{62} & C_{63} & C_{64} & C_{65} & C_{66}
 \end{array}$$

This is equivalent to positiveness of all the principal minors of this matrix (principal minors are square submatrices symmetrical with respect to the main diagonal – they are indicated by dashed lines in the scheme above). All diagonal elastic constants C_{ii} are principal minors, and, therefore, must be positive for all stable crystals. Mechanical stability criteria were first suggested by Max Born (Born and Huang, 1954) and are sometimes called Born conditions. In general form, they are analyzed in detail in Sirotnin and Shaskolskaya (1982) and Fedorov (1968), and cases of different symmetries have been thoroughly analyzed by Cowley (1976) and by Terhune *et al.* (1985). Mechanical stability criteria for crystals under stress must employ the C_{ij} derived from the stress–strain relations (Wang *et al.*, 1993, 1995; Karki, 1997). Violation of any of the mechanical stability conditions leads to softening of an acoustic mode in the vicinity of the Γ -point, inducing a phase transition.

2.06.2.2.3 Birch's law and effects of temperature on the elastic constants

The famous Birch's law (Birch, 1952, 1961; Poirier, 2000) states that compressional sound velocities depend only on the composition and density of the material:

$$v_p = a(\bar{M}) + b(\bar{M})\rho \quad [134]$$

where \bar{M} is the average atomic mass, a and b constants, ρ the density. Thus, for the mantle materials (average atomic mass between 20 and 22),

$$v_p = -1.87 + 3.05\rho \quad [135]$$

Similar relations hold for the bulk sound velocity $v_\Phi = \sqrt{K/\rho}$; for mantle compositions

$$v_\Phi = -1.75 + 2.36\rho \quad [136]$$

Birch's law implies that for a given material at constant volume, the elastic constants are temperature independent. This can be accepted only as a first (strictly harmonic) approximation. Thermal contributions to the bulk modulus can be represented as additive corrections to the zero-temperature result:

$$\begin{aligned}
 K^T(V, T) &= K_{0K}(V) + \Delta K^T_{\text{qha}}(V, T) \\
 &\quad + \Delta K^T_a(V, T)
 \end{aligned} \quad [137]$$

$$\Delta K^T_{\text{qha}}(V, T) = p_{\text{th,qha}}(1 + \gamma - q) - \gamma^2 TC_V/V \quad [138]$$

$$\Delta K^T_a(V, T) = p_a(1 + \gamma_a - q_a) \quad [139]$$

where

$$p_a = \gamma_a E_a/V, \quad \gamma_a = -\left(\frac{\partial \ln a}{\partial \ln V}\right)_T, \quad q_a = \left(\frac{\partial \ln \gamma_a}{\partial \ln V}\right)_T$$

For the adiabatic bulk modulus

$$\begin{aligned}
 K^S(V, T) &= K_{0K}(V) + p_{\text{th,qha}}(1 + \gamma - q) \\
 &\quad + p_a(1 + \gamma_a - q_a)
 \end{aligned} \quad [140]$$

These results can be generalized for the individual elastic constants. Garber and Granato (1975), differentiating the free energy, expressed in the QHA as a sum of mode contributions over the whole Brillouin zone:

$$F = E_{\text{st}} + \frac{1}{2} \sum_{i,\mathbf{k}} \hbar \omega_{i\mathbf{k}} + \sum_{i,\mathbf{k}} k_B T \ln \left[1 - \exp\left(-\frac{\hbar \omega_{i\mathbf{k}}}{k_B T}\right) \right]$$

and obtained the following result, which can be used in calculations of the elastic constants at finite temperatures:

$$\frac{1}{V} \left(\frac{\partial^2 F}{\partial \eta_{ij} \partial \eta_{kl}} \right)_V = \frac{1}{V} \left(\frac{\partial^2 E_{st}}{\partial \eta_{ij} \partial \eta_{kl}} \right)_v + \frac{1}{V} \sum_{i,k} \times \left[\left(\gamma_{ij}^{ik} \gamma_{kl}^{ik} - \frac{\partial \gamma_{ij}}{\partial \eta_{kl}} \right) E_{vib,ik} - \gamma_{ij}^{ik} \gamma_{kl}^{ik} C_{V,ik} T \right] \quad [141]$$

2.06.2.2.4 Elastic anisotropy in the Earth's interior

While most of the lower mantle and the entire outer core are elastically isotropic, seismological studies have indicated seismic anisotropy amounting to a few percent in the upper mantle, lowermost mantle (D'' layer), and in the inner core. This anisotropy can be due to lattice-preferred orientation (e.g., appearing due to plastic flow orienting crystallites in a rock), or due to their reasons such as shape-preferred orientation or macroscopic-scale ordered arrangements of crystals of different minerals and/or molten rock. The most directly testable case is lattice-preferred orientation. Elastic anisotropy causes splitting of seismic waves – much akin to birefringence of light waves in anisotropic crystals. For an overview, see Anderson (1989).

One would expect that crystals will orient their easiest plastic slip planes parallel to the direction of the plastic flow (e.g., in convective streams). The selection of a single dominant slip plane is, of course, a simplification – which, however, leads to a most useful model of a transversely isotropic aggregate (where crystallites have parallel slip planes, but within the slip plane their orientations are random). For the case of a transversely isotropic aggregate with a small degree of anisotropy, Montagner and Nataf (1986) considered the following parameters (the unique axis of the transversely isotropic aggregates is set to be *c*-axis):

$$\begin{aligned} A &= \frac{3}{8}(C_{11} + C_{22}) + \frac{1}{4}C_{12} + \frac{1}{2}C_{66} \\ C &= C_{33} \\ F &= \frac{1}{2}(C_{13} + C_{23}) \\ L &= \frac{1}{2}(C_{44} + C_{55}) \\ N &= \frac{1}{8}(C_{11} + C_{22}) - \frac{1}{4}C_{12} + \frac{1}{2}C_{66} \end{aligned} \quad [142]$$

From these, they derived the velocities of the shear vertically (v_{SV}) and horizontally (v_{SH}), and

compressional vertically (v_{pV}) and horizontally (v_{pH}) polarized waves:

$$\begin{aligned} v_{pH} &= \sqrt{\frac{A}{\rho}}, & v_{pV} &= \sqrt{\frac{C}{\rho}} \\ v_{sH} &= \sqrt{\frac{N}{\rho}}, & v_{sV} &= \sqrt{\frac{L}{\rho}} \end{aligned} \quad [143]$$

What determines the dominant slip system? Strictly speaking, the dislocations – their number and the activation energy for their migration – should be the smallest for the best slip system. However, on the example of h.c.p.-metals, Legrand (1984) has demonstrated that a simplified criterion works very well. The product of the stacking fault enthalpy γ calculated per area $S_{sf}(\gamma = \Delta H_{sf}/S_{sf})$ and the shear elastic constant relevant for the motion of this stacking fault is smallest for the preferred slip plane. For example, comparing basal $\{0001\}$ and prismatic $\{10\bar{1}0\}$ slip for h.c.p.-metals, the ratio

$$R = \frac{\gamma_{0001} C_{44}}{\gamma_{10\bar{1}0} C_{66}} \quad [144]$$

is greater than 1 in cases of prismatic slip and smaller than 1 for materials with basal slip. This criterion was used by Poirier and Price (1999) in their study of the anisotropy of the inner core and, in an extended form, by Oganov *et al.* (2005b) in their revision of the nature of seismic anisotropy of the Earth's D'' layer (see also Section 2.06.4.2).

2.06.3 Phase Transitions of Crystals

The study of phase transitions is of central importance to modern crystallography, condensed matter physics, and chemistry. Phase transitions are a major factor determining the seismic structure of the Earth and thus play a special role in geophysics (e.g., Ringwood, 1991).

2.06.3.1 Classifications of Phase Transitions

A popular classification of phase transitions was proposed by Ehrenfest in 1933 (for a historical and scientific discussion, see Jaeger (1998)), distinguishing between first-, second-, and higher-order phase transitions. For the 'first-order' transitions the 'first' derivatives of the free energy with respect to *P* and *T* (i.e., volume and entropy) are discontinuous at the transition point; for 'second-order' transitions the 'second' derivatives (compressibility, heat capacity, and thermal expansion)

are discontinuous, and so forth. In some cases, the order of the same phase transition is different at different P - T conditions: isosymmetric transitions must be first order, but become completely continuous (infinite-order) transitions at and above the critical temperature. Some transitions change under pressure/temperature from first to second order; the crossover point is called the tricritical point. Among the examples of systems with tricritical crossover are NH_4Cl (Garland and Weiner, 1971), zone-center cubic-tetragonal transition in BaTiO_3 perovskite, possibly the transition from calcite to metastable calcite (II) in CaCO_3 (see Hatch and Merrill (1981)) and, possibly the α - β transition in quartz (SiO_2). For example, the order-disorder transition in NH_4Cl from a phase with a complete orientational disordering of the NH_4 -group ($Pm\bar{3}m$) to an ordered phase ($P4\bar{3}m$) is first order at 1 atm and 242 K, but becomes second order at the tricritical point, 0.15 GPa and 256 K. Therefore, the order of the transition is not something fundamentally inherent to the transition.

The first structural classification was due to Buerger (1961), who distinguished two main types of phase transitions – those with and without changes of the first coordination number, respectively. Each of these types was further classified into reconstructive (i.e., requiring formation/breaking of bonds), displacive, order-disorder, electronic, etc., transitions.

Even though Buerger's classification is purely structural, it naturally gives some insight into thermodynamics and kinetics of phase transitions. For instance, reconstructive transitions are first order and require activation (and, hence, are kinetically controlled) (Polymorphs of carbon (graphite, diamond) and Al_2SiO_5 (minerals kyanite, andalusite, and sillimanite, see Kerrick (1990)) are classical examples. All the transitions between these minerals are first-order reconstructive and require substantial activation energies to proceed; therefore, all the three minerals can coexist at not very high temperatures for millions of years in nature.) Also, as recognized by L. D. Landau in 1937 (see Landau and Lifshitz, 1980), for a second-order transition the two phases must be structurally related, and their symmetry groups must conform to certain group-subgroup relations.

2.06.3.2 First-Order Phase Transitions

Thermodynamics of first-order transitions are based on the Clausius-Clapeyron relation:

$$\frac{dP}{dT} = \frac{\Delta S}{\Delta V} \quad [145]$$

where ΔS and ΔV are the entropy and volume differences, respectively, between the phases. Using [145] one can calculate the slopes of the equilibrium lines of phase coexistence. This relation is valid only for first-order transitions, because for second-order transitions both ΔV and ΔS are equal to zero. The transition temperatures and pressures can be found from accurate atomistic or quantum-mechanical total energy calculations (e.g., Alfè *et al.*, 1999; Oganov *et al.*, 2003, 2005a; Oganov and Ono, 2004, 2005; Umemoto *et al.*, 2006). Only when the two phases are structurally similar can one apply approximate analytical theories, such as Landau theory (which was initially devised to study second-order phase transitions).

A relation, analogous to [145], for second-order transitions was derived by Ehrenfest:

$$\frac{dP}{dT} = \frac{\Delta C_p}{TV\Delta\alpha} \quad [146]$$

where ΔC_p and $\Delta\alpha$ are the jumps of the heat capacity and thermal expansion at the transition. However, precise experiments, computer simulations, and accurate theories indicate a qualitatively different behavior of the heat capacity – instead of having a finite jump, it logarithmically diverges to infinity on both sides of the transition. This 'lambda-behavior' invalidates the Ehrenfest relation.

2.06.3.3 Landau Theory of First- and Second-Order Transitions

When the structural changes occurring upon transition are small, it is usually possible to define an order parameter (or several order parameters), whose continuous change describes all the intermediate structures on the transition pathway. The simplest expression for the free energy is the Landau potential

$$G(Q) = G_0 + \frac{1}{2}A(T - T_C)Q^2 + \frac{1}{3}BQ^3 + \frac{1}{4}CQ^4 + \dots \quad [147]$$

where T_C is the critical temperature, and G_0 the free energy of the phase with $Q=0$ (e.g., high-temperature high-symmetry disordered phase). Landau's assumption that the second term of [147] is simply proportional to $(T - T_C)$ was analyzed and justified mathematically by Sposito (1974). The entropy as a function of the order parameter is simply

$S(Q) = -\partial G(Q)/\partial T = S_0 - (1/2)AQ^2$. This dependence of the entropy on the order parameter is most appropriate for displacive phase transitions. (For order-disorder transitions, the entropy is more accurately expressed as $S(Q) = S_0 - R[(1+Q)\ln(1+Q) + (1-Q)\ln(1-Q)]$.) The internal energy is then $E(Q) = E_0 - (1/2)AT_CQ^2 + (1/3)BQ^3 + (1/4)CQ^4 + \dots$. In the case $A > 0, B > 0, C > 0$, this corresponds to a double-well potential $E(Q)$. (More than two minima can exist for higher-order polynomials [147].) For second-order transitions the odd-order terms in [147] must be zero, making the double well symmetric. (This is only one of the necessary conditions. Other necessary conditions were formulated by Birman (1966) using group theory.)

Consider a second-order transition

$$G(Q) = G_0 + \frac{1}{2}A(T - T_C)Q^2 + \frac{1}{4}CQ^4 + \dots \quad [148]$$

One can observe that at the transition point ($T = T_C, Q = 0$) the second derivative of F with respect to Q changes sign, corresponding to freezing in of a soft mode below T_C and a corresponding structural distortion. For first-order transitions, complete mode softening does not occur at $T = T_C$.

Second-order phase transitions are always characterized by group-subgroup relations: the symmetry group of one ('ordered', usually low-temperature) phase is a subgroup of the symmetry group of the other ('disordered', usually high-temperature) phase. The two symmetrically equivalent minima then correspond to the same ordered phase, and can be considered as 'twin domains', related by a symmetry element present in the disordered phase, but absent in the ordered one (Figure 8).

The potential [147] is often complicated by the coupling of the order parameter to lattice strains. In such cases, the potential will be

$$G(Q) = \left(G_0 + \frac{1}{2}A(T - T_C)Q^2 + \frac{1}{3}BQ^3 + \frac{1}{4}CQ^4 + \dots \right) + a_1Q\varepsilon + a_2Q\varepsilon^2 + a_3Q^2\varepsilon + \frac{1}{2}C\varepsilon^2 + \dots \quad [149]$$

where a_1, a_2, a_3 are coupling coefficients, and C is an elastic constant. Coupling of the order parameter to strains can cause a first-order behavior even for a symmetric $E(Q)$.

In some cases, more than one order parameter is required to describe a phase transition. Then, for the

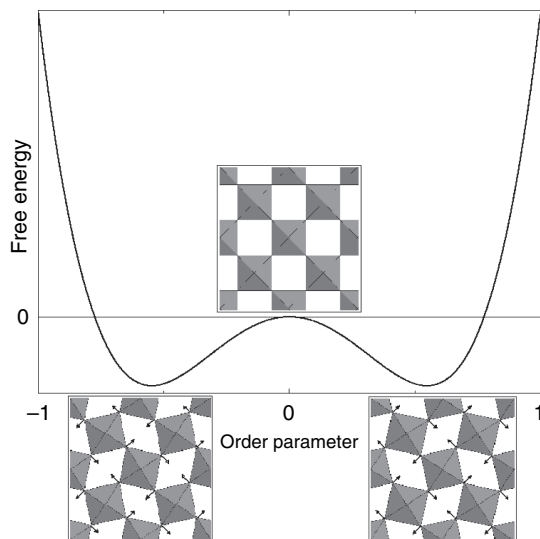


Figure 8 Symmetric Landau potential at $T < T_C$. The two distorted perovskite-type structures shown on the bottom are equivalent (they are mirror reflections of each other); arrows show the directions of octahedral rotations away from the cubic structure. The undistorted structure is shown in the center. At temperatures higher than T_C , the stable structure will be locally distorted, but on average will have the symmetry of the undistorted phase. From Oganov AR, Brodholt JP, and Price GD (2002) *Ab initio* theory of thermoelasticity and phase transitions in minerals. In: Gramaccioli CM (ed.) *EMU Notes in Mineralogy, Vol. 4: Energy Modeling in Minerals*, pp. 83–170. Bolin: Springer.

case of two order parameters, the Landau potential looks like

$$G(Q) = G(Q_1) + G(Q_2) + \xi_1 Q_1 Q_2 + \xi_2 Q_1^2 Q_2 + \xi_3 Q_1 Q_2^2 + \dots \quad [150]$$

where ξ_1, ξ_2 , and ξ_3 are coupling coefficients for the Q_1 - Q_2 coupling. In cases where odd-order terms of the kind $\xi Q_1 Q_2 Q_3$ are present, the transition must be first order. For a detailed general account of Landau theory, see Landau and Lifshitz (1980), Dove (1993, 1997), Carpenter *et al.* (1998), and Carpenter and Salje (1998, 2000).

2.06.3.4 Shortcomings of Landau Theory

Landau theory belongs to a class of approximate theories known as mean-field theories. Mean-field treatment is a common way of approximately solving complex physical problems in many areas of science. The main drawback of these methods is the neglect of short-range fluctuations (in Landau theory, the local structure and fluctuations of the order parameter are neglected). In other words, Landau

theory assumes that all the neighboring unit cells have the same configuration; therefore, domain structures and fluctuations of the order parameter in space and time are not treated. This problem becomes severe in the vicinity of T_C (in the so-called Ginzburg interval). For second-order transitions Landau theory predicts $Q \sim (T_C - T)^{1/2}$, while experiments indicate $Q \sim (T_C - T)^{1/3}$. The critical exponent of 1/3 has been confirmed many times by numerical computer simulations and could be explained only with the advent of renormalization group theory. (In fact, experiments give mean-field critical exponents far from T_C , but nearer T_C there is crossover from the mean-field to critical behavior, where the critical exponents depart significantly from mean-field predictions.) Landau theory cannot explain the logarithmic divergence of the heat capacity near the critical point – instead, it yields a finite jump. Finally, Landau theory does not consider quantum effects at low temperatures. As a consequence, it does not reproduce experimentally observed order parameter saturation at low temperatures; instead, it predicts a steady increase of the order parameter with decreasing temperature.

2.06.3.5 Ginzburg–Landau Theory

In 1950, V. L. Ginzburg and L. D. Landau (see Landau and Lifshitz (1980) and Bowley and Sánchez (1999)) considered the case of an order parameter slowly varying in space. This leads to the simplest theory beyond the mean field. The free energy becomes a ‘functional’ of the order parameter, and an additional term proportional to the square of the gradient of the order parameter appears:

$$F[Q(\mathbf{r})] = \int \left\{ f(Q(\mathbf{r})) + \frac{1}{2} \lambda [\nabla Q(\mathbf{r})]^2 \right\} d\mathbf{r} \quad [151]$$

with the stiffness parameter $\lambda > 0$. For example, for a second-order transition

$$F[Q(\mathbf{r})] = \int \left\{ \frac{1}{2} a(T - T_C) Q^2(\mathbf{r}) + \frac{1}{4} b Q^4(\mathbf{r}) + \frac{1}{2} \lambda [\nabla Q(\mathbf{r})]^2 \right\} d\mathbf{r} \quad [152]$$

The order parameter is then expressed as a sum of a constant term (the average order parameter) and fluctuations, given by a Fourier series:

$$Q(\mathbf{r}) = \bar{Q} + \sum_{\mathbf{k}} Q_{\mathbf{k}} e^{i\mathbf{k}\mathbf{r}} \quad [153]$$

Equation [152] can be rewritten as

$$\begin{aligned} F[Q(\mathbf{r})] &= \int \left\{ f(\bar{Q}) + Q_1(\mathbf{r}) f' \right. \\ &\quad \left. + \frac{1}{2} Q_1^2(\mathbf{r}) f'' + \dots + \frac{1}{2} \lambda [\nabla Q(\mathbf{r})]^2 \right\} d\mathbf{r} \\ &= V \left\{ f(\bar{Q}) + \frac{1}{2} \sum_{\mathbf{k}} |Q_{\mathbf{k}}|^2 (f'' + \lambda k^2) + \dots \right\} \end{aligned} \quad [154]$$

Let us consider the case $f'' < 0$. In this case, the system is unstable against all fluctuations whose wave vectors satisfy $f'' + \lambda k^2 > 0$. Hence, the maximum unstable wave vector is $k_c = \sqrt{|f''|/\lambda}$. The correlation length ξ is

$$\xi = k_c^{-1} = \sqrt{\frac{\lambda}{|f''|}} \quad [155]$$

Ginzburg and Landau have proposed a criterion of the validity of Landau theory, defining the following value:

$$r(T) = \frac{f_m \xi^3}{k_B T} \quad [156]$$

where f_m is the difference of energies at the energy maximum and minimum. If $r(T) > 1$, fluctuations are not important, and Landau theory is valid. When $r(T) < 1$, fluctuations are essential and Landau theory is invalid; this occurs in the vicinity of T_C (in the temperature region called Ginzburg interval). Ginzburg intervals are usually quite narrow (of the order of ~ 10 K).

For second-order transitions, $f_m = a^2(T - T_C)/4b$ and

$$\xi = \sqrt{\frac{\lambda}{2a(T_C - T)}} \quad [157]$$

Ginzburg–Landau theory is still approximate and does not reproduce experimental critical exponents. Renormalization group theory overcomes all these difficulties and serves as the modern basis of theory of critical phenomena; it goes beyond the mean-field approximation and fully treats all possible fluctuations of the order parameter. Introductory texts on this theory can be found in Chandler (1987), Rao and Rao (1978), and Wilson (1983); the latter reference is the Nobel lecture of Kenneth Wilson, one of its main inventors. This theory has led to the prediction of new physical phenomena, for example, continuous lattice melting, experimentally found in Na_2CO_3 (Harris and Dove, 1995).

2.06.3.6 Ising Spin Model

This model is widely used to describe magnetic and atomic ordering processes in materials. In this model, a spin +1 or -1 is associated with each lattice site, depending on whether the magnetic moment on the site is 'up' or 'down', or whether the atom occupying the site is of the type 'A' or 'B'.

The total energy of the system is

$$U = U_0 - \mathcal{J} \sum_{i,j} S_i S_j - H \sum_i S_i \quad [158]$$

where U_0 is the reference energy, and \mathcal{J} the interaction parameter between the sites: if $\mathcal{J} < 0$, unlike spins prefer to group together, and there is a tendency to ordering at low temperatures; if $\mathcal{J} > 0$, unmixing will occur at low temperatures. Complete disorder, although unfavorable energetically, will be stabilized by the entropy at high temperatures. An external field H leads to a preferred orientation of the spins. The Ising model can be analytically solved only in one and two dimensions; for three dimensions it is solved numerically, usually by the Monte Carlo method. One-dimensional Ising model exhibits no phase transitions, and at all temperatures above 0 K yields the disordered state.

Ising-like models provide an interesting route for theoretical studies of polytypism and polysomatism (see, e.g., Price (1983), Price and Yeomans (1984) and references therein). The crucial observation is the mathematical similarity between polytypic sequences (e.g., **Figure 9**) and one-dimensional Ising models.

The Ising model is also very attractive for studies of ordering processes; for a review the reader is referred to Warren *et al.* (2001), and can be generalized for the case of more than two spins (see Yeomans, 1992) – such variants will be applicable to ordering in multicomponent solid solutions and polytypic (polysomatic) systems with more than two types of layers.

The conventional Ising models assume that spins can be only 'up' or 'down', and therefore these models cannot be applied to noncollinear magnetic materials. For these cases, various Heisenberg models are appropriate, which take into account the orientations of the spins. The simplest of these models is based on the following Hamiltonian:

$$U = U_0 - \mathcal{J} \sum_{i,j} \mathbf{S}_i \cdot \mathbf{S}_j - H \sum_i S_i^z \quad [159]$$

involving spin vectors \mathbf{S}_i and \mathbf{S}_j . By analogy with the one-dimensional Ising model, the Heisenberg model

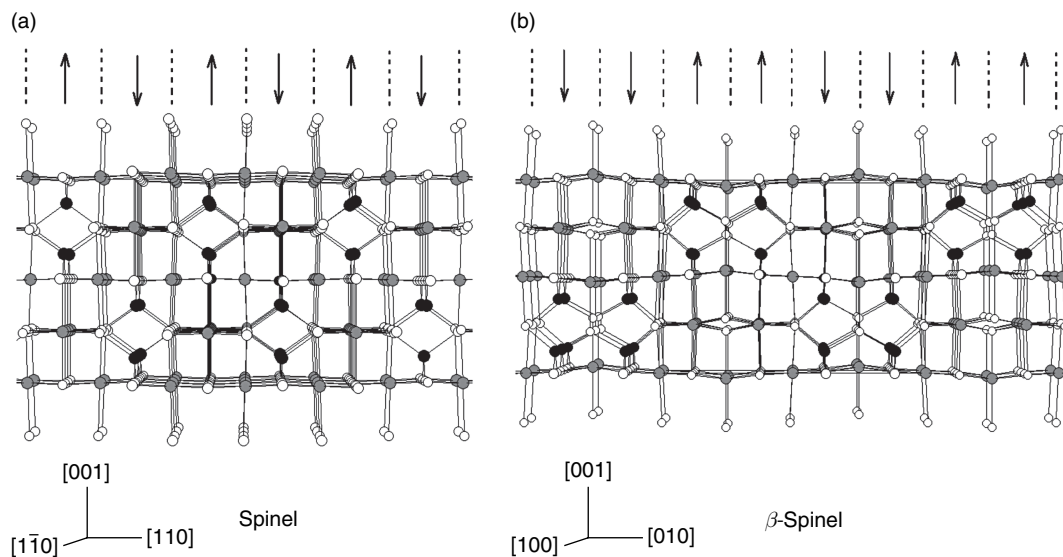


Figure 9 Polytypism in spinelloids. Structures of (a) spinel, (b) wadsleyite (β -spinel). Black circles are Si atoms (tetrahedrally coordinated), gray circles Mg atoms (octahedrally coordinated), and empty circles are O atoms. Layers of different orientations are shown by 'up' and 'down' arrows highlighting the similarity with the one-dimensional Ising spin lattice. Spinelloids are interesting for Earth sciences, because of the phases of Mg_2SiO_4 – ringwoodite (spinel-like phase) and wadsleyite (β -spinel phase), which are the major constituents of the transition zone of the Earth's mantle.

has no phase transitions for one- and two-dimensional systems.

2.06.3.7 Mean-Field Treatment of Order–Disorder Phenomena

The Bragg–Williams model is the simplest mean-field approach applicable to ordering phenomena. The free energy of the alloy as a function of temperature and order parameter is

$$G = G_0 - \frac{Nz}{4} \mathcal{J} Q^2 + Nk_B T [(1 + Q) \ln(1 + Q) + (1 - Q) \ln(1 - Q)] \quad [160]$$

where G_0 is the free energy of the fully disordered state, N is the number of sites where disordering occurs, the order parameter $Q = X_{A,\alpha} - X_{A,\beta} = X_{B,\beta} - X_{B,\alpha} = 2X_{A,\alpha} - 1$, and the exchange energy $\mathcal{J} = E_{AA} + E_{BB} - 2E_{AB}$.

The expression [160] is analogous to the Landau potential [148] and yields the same critical exponents. In three dimensions, this model gives qualitatively reasonable results; however, even with accurate exchange energies \mathcal{J} , the predicted transition temperatures are usually a few times higher than the experimental ones (Redfern, 2000).

Drawbacks of the Bragg–Williams model can be corrected by explicitly considering short-range order. In the Bethe model (see Rao and Rao (1978)), apart from the long-range order parameter Q , one or more short-range order parameters are considered. These additional parameters describe the distribution of neighbors of both kinds in the nearest proximity of each atom. The resulting critical exponents and transition temperatures are much more realistic than mean-field predictions.

In the following, we discuss features of different types of phase transitions, classified by their symmetry. This gives a new viewpoint on the variety of phenomena associated with phase transitions in solids.

2.06.3.8 Isosymmetric Transitions

Using Landau theory, it is easy to show that isosymmetric transitions must be first order, but can disappear (i.e., become fully continuous, infinite-order transitions) above the critical temperature (Bruce and Cowley, 1981; Christy, 1995). There is a complete analogy here with the liquid–gas and liquid–liquid transitions (which are also isosymmetric). All

liquid, gaseous, and conventional amorphous phases are isosymmetric, having spherical point-group symmetry. At supercritical temperatures there are generally rapid, but continuous changes in all properties along any P – T path going above the critical point (Angel, 1996).

Increasingly, many crystals are now known to exhibit isosymmetric phase transitions (i.e., those for which both phases have the same space group with the same number of atoms in the unit cell, with atoms occupying the same Wyckoff positions). Such transitions can be electronic (where the electronic structure changes, e.g., Ce and SmS), structural (where the coordination or ordering of the atomic species change discontinuously, e.g., KTiOPO_4), or intermediate (both electronic and structural changes are involved, e.g., Na_3MnF_6). Metallic Ce undergoes an isosymmetric phase transition Ce(I)–Ce(IV) (see Liu and Bassett (1986) and references therein), presumably due to $6s$ – $4f$ (or $5d$) electronic transition. Both Ce(I) and Ce(IV) have the f.c.c. structure (space group $Fm\bar{3}m$). The volume change at the transition is very large (13%) at room temperature, but it rapidly decreases along the Ce(I)–Ce(IV) equilibrium line until it disappears at the critical point (2.15 GPa and 613 K). Another famous example of an electronic transition is SmS, which transforms from the low-pressure insulating phase to the high-pressure metallic phase; both phases have an NaCl-type structure. Figure 10 explains this transition.

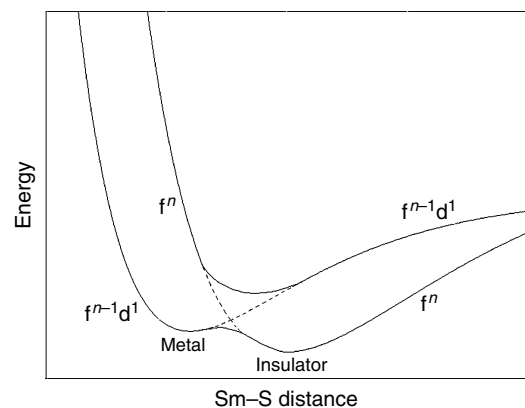


Figure 10 Illustration of the isosymmetric metal–insulator transition in SmS. Mixing of two configurations (metallic $f^{n-1}d^1$ and insulating f^n) produces a double-well energy curve for the ground state, where the minimum with a smaller interatomic distance corresponds to a metal. Compression triggers the insulator–metal transition. Adapted from Burdett JK (1995) *Chemical Bonding in Solids*, 319 pp. New York: Oxford University Press.

Structural isosymmetric transitions do not involve any drastic changes in the electronic structure, but are purely atomistic. KTiOPO_4 (KTP) is known to undergo a phase transition at 5.8 GPa with a volume decrease of 2.7% with preservation of space group $Pna2_1$ (Allan and Nelmes, 1996). Large cages, occupied by K, lose 12% of their volume upon transition. $\text{KNO}_3(\text{II})\text{--KNO}_3(\text{IV})$ phase transition, which occurs at 0.3 GPa and is accompanied by a volume decrease of 11.5%, does not alter the space group ($Pnma$) (Adams *et al.*, 1988), while for potassium atoms the coordination number changes from 9 to 11. An isosymmetric (space group $Pnam$) phase change has been observed at 9.8 GPa for PbF_2 (Haines *et al.*, 1998) and involves a change of the coordination number of Pb atoms from 9 to 10. Na_3MnF_6 (space group $P2_1/n$) is an example of a phase transition with a simultaneous change in the atomic and electronic structure. At 2.2 GPa this compound undergoes a first-order isosymmetric phase transformation, which is associated with a change of orientation of the Jahn–Teller elongation of MnF_6 octahedra (Carlson *et al.*, 1998).

2.06.3.9 Transitions with Group–Subgroup Relations

There are several possibilities here, stemming from different types of subgroups/supergroups of crystal symmetry. Examples are $\alpha\rightarrow\beta$ quartz, $P2_1/c\text{--}C2/c$ pyroxenes (see very interesting papers by Arlt and Angel (2000) and Arlt *et al.* (1998)), and $Pbmm\rightarrow Pm\bar{3}m$ transitions in perovskites.

The second type of transitions with group–subgroup transitions involve indirect symmetry relations between two phases via an intermediate archetypal phase of a higher symmetry, which is a supergroup for symmetries of both phases. An example is BaTiO_3 , where the transition between the rhombohedral and tetragonal phases can be described with reference to the higher-symmetry cubic phase. Such transitions are usually weakly first order.

The third possibility involved a transition state of lower symmetry, which is a common subgroup of the symmetries of both phases. These transitions are usually strongly first order; often they can be described as reconstructive (see Christy (1993)). The f.c.c.→b.c.c. transition in Fe can be described with reference to lower-symmetry tetragonal or rhombohedral configurations, whose symmetries are common subgroups of both symmetry groups of the b.c.c. and f.c.c. phases.

2.06.3.10 Pressure-Induced Amorphization

This phenomenon, discovered in 1984 in experiments on compression of ice (Mishima *et al.*, 1984) to 1 GPa at 77 K, is still poorly understood. For detailed reviews, see excellent papers (Sharma and Sikka, 1996; Richet and Gillet, 1997).

A great number of crystals undergoing pressure-induced amorphization are known (e.g., Quartz SiO_2 , coesite SiO_2 , berlinite AlPO_4 , GeO_2 , zeolites scolecite $\text{Ca}_8\text{Al}_{16}\text{Si}_{24}\text{O}_{80}\cdot 24\text{H}_2\text{O}$ and mesolite $\text{Na}_{16}\text{Ca}_{16}\text{Al}_{48}\text{Si}_{72}\text{O}_{240}\cdot 64\text{H}_2\text{O}$, anorthite $\text{CaAl}_2\text{Si}_2\text{O}_8$, wollastonite CaSiO_3 , enstatite MgSiO_3 , muscovite $\text{KAl}_3\text{Si}_3\text{O}_{10}(\text{OH})_2$, serpentine $\text{Mg}_3\text{Si}_2\text{O}_5(\text{OH})_4$, portlandite $\text{Ca}(\text{OH})_2$), as well as a few substances undergoing pressure-release amorphization, whereby high-pressure phases, when decompressed to pressures well below their stability fields, become dynamically unstable and amorphize. (This happens to the perovskite-type modification of CaSiO_3 , one of the main minerals of the Earth's lower mantle, which at ambient conditions turns to a glass within a few hours.)

Pressure-induced amorphization is always a metastable first-order transition. It occurs in the limit of dynamical stability of the crystal. Behavior of pressure-induced amorphous phases on decompression can be very different: some compounds (e.g., $\text{Ca}(\text{OH})_2$) recrystallize, others (e.g., SiO_2 , ice) remain amorphous. Elastic anisotropy was found in pressure-amorphized quartz by Brillouin spectroscopy (McNeil and Grimsditch, 1991) and molecular dynamics simulations (Tse and Klug, 1993). The latter study found no structural relationships between pressure-amorphized quartz and silica glass.

The mechanisms driving pressure-induced amorphization are still not quite clear. The necessary conditions are (1) higher density of the amorphous phase relative to the crystal and (2) presence of soft modes in the crystalline phase. Softening of a vibrational mode at a single point of the Brillouin zone should drive a transition to a crystalline (if the soft wave vector is rational) or incommensurate (if the wave vector is irrational) phase. Simultaneous or nearly simultaneous softening of a phonon branch at a range of k -vectors could produce an amorphous phase (Keskar *et al.*, 1994; Binggeli *et al.*, 1994; Hemmati *et al.*, 1995). Any atomic displacement, expressible as a combination of soft modes, lowers the energy; the multitude of possible combinations gives rise to the disorder. However, a large degree of order should remain because the displacements are expected to be small and because only displacements

related to the softening phonon branch are allowed to freeze in. Simultaneous softening of a phonon branch along a direction in the Brillouin zone implies weak dispersion of this branch, which is most naturally achieved when the unit cell is large. Indeed, crystals with complicated open structures and large unit cells are more prone to pressure-induced amorphization.

2.06.4 A Few Examples of the Discussed Concepts

Very briefly, we will discuss some recent results illustrating the use of the notions and theories discussed above. These include the calculation of the temperature profile of the Earth's lower mantle and core, polytypism of MgSiO₃ post-perovskite and seismic anisotropy of the Earth's D'' layer, and spin transition in (Mg, Fe)O magnesio-wüstite.

2.06.4.1 Temperature Profile of the Earth's Lower Mantle and Core

Equation [26] can be rewritten, taking into account eqn [85b], as follows:

$$\left(\frac{\partial \ln T}{\partial \rho}\right)_s = \gamma_\alpha \quad [161]$$

This formula describes adiabatic change of temperature upon compression and is relevant for first-order estimates of the average temperature distribution in convecting mantle (where superadiabatic effects might be non-negligible) and outer core (which is very closely adiabatic). *Ab initio* calculations of Alfè *et al.* (2002) produced an estimate of the temperature at the inner–outer core boundary (5150 km depth) of 5600 K. This was calculated from the melting curve of iron, taking into account the effect of impurities (Si, S, O). While within the solid inner core the temperature is likely to be constant, the temperature distribution in the liquid and rapidly convecting outer core is adiabatic [161]. With their estimates of the Grüneisen parameter of liquid iron at relevant pressures and temperatures, Alfè *et al.* (2002) calculated the temperature distribution in the outer core. In particular, the core temperature at the boundary with the mantle was estimated to be in the range 4000–4300 K.

Phase-equilibrium experiments of Ito and Katsura (1989) produced another ‘anchor’ point for the calculation of the geotherm – 1873 K at the depth of

670 km (top of the lower mantle). Taking into account the Grüneisen parameters of MgSiO₃ perovskite and MgO periclase obtained in their *ab initio* simulations. Oganov *et al.* (2002) have calculated the adiabatic geotherm of the lower mantle. The resulting mantle temperature at the boundary with the core (2891 km depth) is 2700 K, indicating a strong thermal boundary layer with large temperature variations at the bottom of the mantle. Lateral temperature variations in the lower mantle have been estimated (Oganov *et al.*, 2001a) by combining seismic tomography images and computed elastic constants of MgSiO₃ perovskite as a function of pressure and temperature (Oganov *et al.*, 2001a). These variations were found to increase from 800 K at the depth of 1000 km to ~2000 K close to the bottom of the lower mantle.

2.06.4.2 Polytypism of MgSiO₃ Post-Perovskite and Anisotropy of the Earth's D'' layer

The original findings of the post-perovskite phase of MgSiO₃ (Murakami *et al.*, 2004; Oganov and Ono, 2004) came as a big surprise. The unusual crystal structure of post-perovskite and its elastic properties naturally explained most of the anomalies of the D'' layer – the D'' discontinuity and its variable depth, the anticorrelation of shear and bulk sound velocities and seismic anisotropy of the D'' layer (see Oganov and Ono (2004), Murakami *et al.* (2004), and Oganov *et al.* (2005b)).

Recently, Oganov *et al.* (2005b) found that MgSiO₃ perovskite and post-perovskite can be considered as end members of an infinite polytypic series (Figure 11) – this is a case of nontraditional polytypism (for another illustration, see Figure 9), since the ‘layers’, whose shifting produces all the structures in the polytypic series, are not weakly bound and are not even immediately obvious in the structure. All these structures are energetically very similar, and since intermediate structures have only marginally higher enthalpies than perovskite or post-perovskite, these phases could be stabilized by temperature and/or impurities in the Earth's lowermost mantle. This polytypism with low-energy stacking faults has interesting implications for plasticity of MgSiO₃ post-perovskite and for seismic anisotropy of the D'' layer.

Initially, {010} slip planes parallel to the silicate sheets of the post-perovskite structure were expected

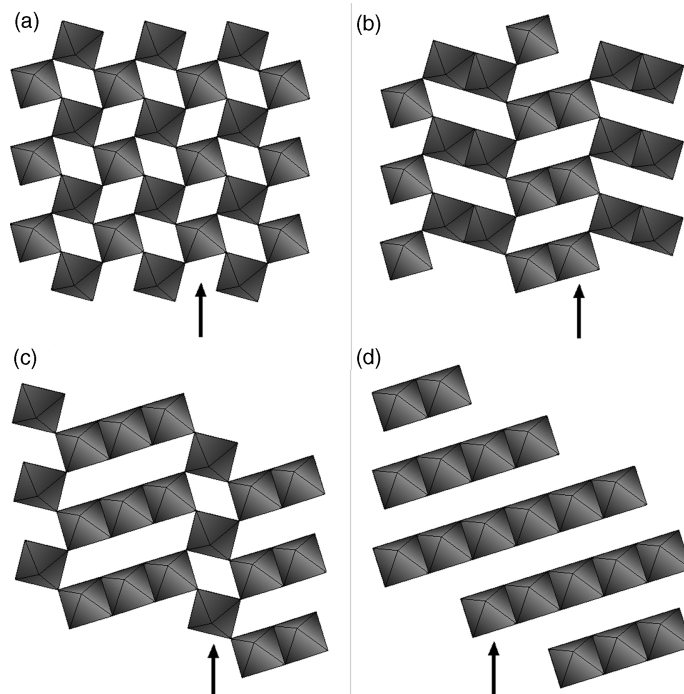


Figure 11 MgSiO₃ polytypes: (a) Perovskite (space group $Pbnm$); (b) and (c) intermediate structures 2×2 ($Pbnm$) and 3×1 ($P2_1/m$), respectively and (d) post-perovskite ($Cmcm$). Only silicate octahedra are shown; Mg atoms are omitted for clarity. Arrows indicate the predicated slip planes in these structures. From Oganov AR, Martoňák R, Laio A, Raiteri P, and Parrinello M (2005b) Anisotropy of Earth's D'' layer and stacking faults in the MgSiO₃ post-perovskite phase. *Nature* 438: 1142–1144.

to be dominant in post-perovskite. However, *ab initio* simulations (Oganov *et al.*, 2005b) found that the {110} slip planes are much more favorable. In particular, this conclusion was supported by applying Legrand's criterion – generalization of eqn [144]. With these slip planes and using the method of Montagner and Nataf (1986), eqns [142] and [143], one obtains a more consistent interpretation of seismic anisotropy of the D'' layer than with the {010} slip planes. In particular, much smaller degrees of lattice-preferred orientation are needed to explain the observed seismic anisotropy and there is now a possibility to explain the observed (Garnero *et al.*, 2004; Wookey *et al.*, 2005) inclined character of anisotropy. Subsequent radial diffraction experiments on analog MgGeO₃ post-perovskite (Merkel, personal communication) have confirmed the prediction of Oganov *et al.* (2005b) on the dominant role of the {110} slip planes in MgSiO₃ post-perovskite. Furthermore, recent seismological studies (Wookey, personal communication) found that only {110} slip is consistent with observations.

2.06.4.3 Spin Transition in (Mg, Fe)O Magnesiowüstite

Iron impurities play a large role in determining the properties of Earth-forming minerals. One particular complication arising from the presence of these impurities is the possible pressure-induced transition of Fe²⁺ (or Fe³⁺) impurities from the high-spin into the low-spin state. Typically, crystal fields induced by the O²⁻ ions at low pressures are weak, and transition metal ions prefer to adopt the high-spin configurations (like in free ions). However, under pressure the increasing crystal field and the additional PV term in the free energy prompt these ions to adopt much more compact low-spin forms (it is well documented that ionic radii are much larger for high-spin ions than for low-spin ones – for example, Shannon and Prewitt (1969). Recent studies of such a transition in (Mg, Fe)O magnesiowüstite (Badro *et al.*, 2003; Lin *et al.*, 2005) demonstrated that this transition might have large effects on physical properties of minerals.

This spin transition is isosymmetric, and as such it must (see Section 2.06.3) be first-order at low temperatures and fully continuous above some critical temperature T_{cr} . While at 0 K the low-pressure phase will contain only high-spin Fe^{2+} ions, and only low-spin ions will be present in the high-pressure phase, on increasing temperature there will be an increased degree of coexistence of the two spin states in the same phase – as a consequence, the first-order character of the transition decreases with temperature. At T_{cr} the miscibility of high- and low-spin ions become complete and the transition becomes fully continuous (infinite order, rather than first or second order); T_{cr} is proportional to the enthalpy that arises from the deformation of the structure due to insertion of a ‘wrong’-spin ion. While quantitative aspects of this transition are actively studied by several groups, the most important qualitative features (in addition to those mentioned above) are immediately clear:

1. Large positive Clapeyron slope (since at high temperatures magnetic entropy is large for high-spin Fe^{2+} and zero for low-spin Fe^{2+}).
2. Low T_{cr} , perhaps several hundred kelvin, since for relevant compositions (e.g. $\text{Mg}_{0.8}\text{Fe}_{0.2}\text{O}$) the energetic effects of Fe incorporation and the enthalpy of ‘spin mixing’ will be rather small.

At lower-mantle temperatures the transition is likely to be continuous. A schematic phase diagram is

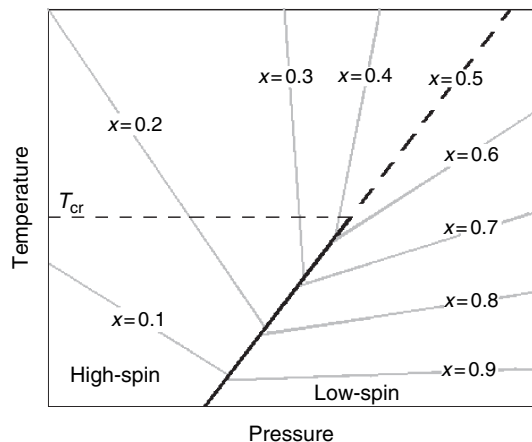


Figure 12 Schematic phase diagram for a system with a spin transition, for example, $(\text{Mg,Fe})\text{O}$. Thick solid line indicates first-order transition, and thick dashed line indicates continuous transition. Gray lines show the degree of spin miscibility (numbers: concentration of low-spin species relative to the total number of iron atoms). Above T_{cr} the transition is fully continuous.

shown in **Figure 12**. Simplified theory of the spin transition in $(\text{Mg, Fe})\text{O}$ was developed by Sturhahn *et al.* (2005).

References

- Ackland GJ and Reed SK (2003) Two-band second moment model and an interatomic potential for caesium. *Physical Review B* 67: 174108.
- Adams DM, Hatton PD, Heath AE, and Russell DR (1988) X-ray diffraction measurements on potassium nitrate under high pressure using synchrotron radiation. *Journal of Physics C* 21: 505–515.
- Al'tshuler LV, Brusnikin SE, and Kuzmenkov EA (1987) Isotherms and Grüneisen functions of 25 metals. *Journal of Applied Mechanics and Technical Physics* 161: 134–146.
- Alexandrov KS and Prodaivoda GT (1993) Elastic properties of minerals. *Crystallografiya* 38: 214–234 (in Russian).
- Alfè D, Gillan MJ, and Price GD (1999) The melting curve of iron at the pressures of the Earth's core from *ab initio* calculations. *Nature* 401: 462–464.
- Alfè D, Gillan MJ, and Price GD (2002) Composition and temperature of the Earth's core constrained by combining *ab initio* calculations and seismic data. *Earth and Planetary Science Letters* 195: 91–98.
- Allan DR and Nelmes RJ (1996) The structural pressure dependence of potassium titanyl phosphate (KTP) to 8 GPa. *Journal of Physics – Condensed Matter* 8: 2337–2363.
- Allen MP and Tildesley DJ (1987) *Computer Simulation of Liquids*, 385 pp. Oxford: Clarendon Press.
- Anderson DL (1989) *Theory of the Earth*, 366 pp. Boston: Blackwell.
- Angel RJ (1996) New phenomena in minerals at high pressures. *Phase Transitions* 59: 105–119.
- Angel RJ, Allan DR, Milletich R, and Finger LW (1997) The use of quartz as an internal pressure standard in high-pressure crystallography. *Journal of Applied Crystallography* 30: 461–466.
- Arlt T and Angel RJ (2000) Displacive phase transitions in C-centred clinopyroxenes: Spodumene, $\text{LiScSi}_2\text{O}_6$ and ZnSiO_3 . *Physics and Chemistry of Minerals* 27: 719–731.
- Arlt T, Angel RJ, Milletich R, Armbruster T, and Peters T (1998) High-pressure $P2_1/c$ - $C2/c$ phase transitions in clinopyroxenes: Influence of cation size and electronic structure. *American Mineralogist* 83: 1176–1181.
- Badro J, Fiquet G, Guyot F, *et al.* (2003) Iron partitioning in Earth's mantle: Toward a deep lower mantle discontinuity. *Science* 300: 789–791.
- Baroni S, de Gironcoli S, Dal Corso A, and Gianozzi P (2001) Phonons and related crystal properties from density-functional perturbation theory. *Reviews of Modern Physics* 73: 515–562.
- Baroni S, Gianozzi P, and Testa A (1987) Green-function approach to linear response in solids. *Physical Review Letters* 58: 1861–1864.
- Barron THK and Klein ML (1965) Second-order elastic constants of a solid under stress. *Proceedings of the Physical Society* 85: 523–532.
- Belikov BP, Aleksandrov KS, and Ryzhova TV (1970) *Elastic Constants of Rock-Forming Minerals*, 276 pp. Moscow: Nauka (in Russian).
- Binggeli N, Keskar NR, and Chelikowsky JR (1994) Pressure-induced amorphisation, elastic instability, and soft modes in α -quartz. *Physical Review B* 49: 3075–3081.
- Birch F (1952) Elasticity and constitution of the Earth's interior. *Journal of Geographical Research* 57: 227–286.

- Birch F (1961) Composition of the Earth's mantle. *Geophysical Journal of the Royal Astronomical Society* 4: 295–311.
- Birman JL (1966) Simplified theory of symmetry change in second-order phase transitions: Application to V_3Si . *Physical Review Letters* 17: 1216–1219.
- Born M and Huang K (1954) *Dynamical Theory of Crystal Lattices*, 420 pp. Oxford: Oxford University Press.
- Bowler R and Sánchez M (1999) *Introductory Statistical Mechanics*, 2nd edn., 352 pp. Oxford: Oxford University Press.
- Bruce AD and Cowley RA (1981) *Structural Phase Transitions*, 326 pp. London: Taylor and Francis.
- Burger MJ (1961) Polymorphism and phase transformations. *Fortschritte Der Mineralogie* 39: 9–24.
- Bukowski MST (1994) Quantum geophysics. *Annual Reviews of Earth and Planetary Science* 22: 167–205.
- Burdett JK (1995) *Chemical Bonding in Solids*, 319 pp. New York: Oxford University Press.
- Carlson S, Xu YQ, Halenius U, and Norrestam R (1998) A reversible, isosymmetric, high-pressure phase transition in Na_3MnF_6 . *Inorganic Chemistry* 37: 1486–1492.
- Carpenter MA and Salje EKH (1998) Elastic anomalies in minerals due to structural phase transitions. *European Journal of Mineralogy* 10: 693–812.
- Carpenter MA and Salje EKH (2000) Strain and Elasticity at Structural Phase Transitions in Minerals. *Reviews in Mineralogy and Geochemistry* 39: 35–64.
- Carpenter MA, Salje EKH, and Graeme-Barber A (1998) Spontaneous strain as a determinant of thermodynamic properties for phase transitions in minerals. *European Journal of Mineralogy* 10: 621–691.
- Catti M (1989) Crystal elasticity and inner strain – A computational model. *Acta Crystallographica A* 45: 20–25.
- Chandler D (1987) *Introduction to Modern Statistical Mechanics*, 274 pp. NY: Oxford University Press.
- Christy AG (1993) Multistage diffusionless pathways for reconstructive phase transitions: application to binary compounds and calcium carbonate. *Acta Crystallographica B* 49: 987–996.
- Christy AG (1995) Isosymmetric structural phase transitions: Phenomenology and examples. *Acta Crystallographica B* 51: 753–757.
- Cohen RE, Gulseren O, and Hemley RJ (2000) Accuracy of equation-of-state formulations. *American Mineralogist* 85: 338–344.
- Cowley RA (1976) Acoustic phonon instabilities and structural phase transitions. *Physical Review B* 13: 4877–4885.
- Dove M (2003) *Structure and Dynamics*. Oxford: Oxford University Press.
- Dove MT (1993) *Introduction to Lattice Dynamics*, 258 pp. Cambridge: Cambridge University Press.
- Dove MT (1997) Theory of displacive phase transitions in minerals. *American Mineralogist* 82: 213–244.
- Fedorov FI (1968) *Theory of Elastic Waves In Crystals*, 375 pp. New York: Plenum.
- Gale JD (1998) Analytical free energy minimization of silica polymorphs. *Journal of Physical Chemistry B* 102: 5423–5431.
- Garber JA and Granato AV (1975) Theory of the temperature dependence of second-order elastic constants in cubic materials. *Physical Review B* 11: 3990–3997.
- Garland CW and Weiner BB (1971) Changes in the thermodynamic character of the NH_4Cl order–disorder transition at high pressures. *Physical Review B* 3: 1634–1637.
- Garnero EJ, Maupin V, Lay T, and Fouch MJ (2004) Variable azimuthal anisotropy in Earth's lowermost mantle. *Science* 306: 259–261.
- Gillet P, Matas J, Guyot F, and Ricard Y (1999) Thermodynamic properties of minerals at high pressures and temperatures from vibrational spectroscopic data. In: Wright K and Catlow R (eds.) *Microscopic Properties and Processes in Minerals*, NATO Science Series, v. C543, pp. 71–92. Dordrecht: Kluwer.
- Haines J, Leger JM, and Schulte O (1998) High-pressure isosymmetric phase transition in orthorhombic lead fluoride. *Physical Review B* 57: 7551–7555.
- Hama J and Suito K (1996) The search for a universal equation of state correct up to very high pressures. *Journal of Physics – Condensed Matter* 8: 67–81.
- Harris MJ and Dove MT (1995) Lattice melting at structural phase transitions. *Modern Physics Letters* 9: 67–85.
- Hatch DM and Merrill L (1981) Landau description of the calcite– $CaCO_3(II)$ phase transition. *Physical Review B* 23: 368–374.
- Hemmati M, Czizmeshya A, Wolf GH, Poole PH, Shao J, and Angell CA (1995) Crystalline–amorphous transition in silicate perovskites. *Physical Review B* 51: 14841–14848.
- Holzappel WB (1996) Physics of solids under strong compression. *Reports on Progress in Physics* 59: 29–90.
- Holzappel WB (2001) Equations of state for solids under strong compression. *Zeitschrift Fur Kristallographie* 216: 473–488.
- Iannuzzi M, Laio A, and Parrinello M (2003) Efficient exploration of reactive potential energy surfaces using Car–Parrinello molecular dynamics. *Physical Review Letters* 90: (art. no. 238302).
- Hahn Th (ed.) (1994) *International Tables for Crystallography, Vol. A., Space-Group Symmetry*. Dordrecht: Kluwer.
- Ito E and Katsura T (1989) A temperature profile of the mantle transition zone. *Geophysical Research Letters* 16: 425–428.
- Jaeger G (1998) The Ehrenfest classification of phase transitions: Introduction and evolution. *Archives of Histology and Exact Science* 53: 51–81.
- Kantorovich LN (1995) Thermoelastic properties of perfect crystals with nonprimitive lattices: 1: General theory. *Physical Review B* 51: 3520–3534.
- Karki BB (1997) *High-Pressure Structure and Elasticity of the Major Silicate and Oxide Minerals of the Earth's Lower Mantle*, 170 pp. PhD Thesis, University of Edinburgh.
- Karki BB, Wentzcovitch RM, de Gironcoli S, and Baroni S (1999) First-principles determination of elastic anisotropy and wave velocities of MgO at lower mantle conditions. *Science* 286: 1705–1707.
- Karki BB, Wentzcovitch RM, de Gironcoli S, and Baroni S (2000) Ab initio lattice dynamics of $MgSiO_3$ perovskite at high pressure. *Physical Review B* 62: 14750–14756.
- Kerrick DM (1990) The Al_2SiO_5 Polymorphs. *Reviews in Mineralogy* 22: 406.
- Keskar NR, Chelikowsky JR, and Wentzcovitch RM (1994) Mechanical instabilities in $A1PO_4$. *Physical Review B* 50: 9072–9078.
- Kieffer SW (1979) Thermodynamics and lattice vibrations of minerals. 1: Mineral heat capacities and their relationship to simple lattice vibrational models. *Reviews of Geophysics and Space Physics* 17: 1–19.
- Kunc K, Loa I, and Syassen K (2003) Equation of state and phonon frequency calculations of diamond at high pressures. *Physical Review B* 68: (art. 094107).
- Laio A and Parrinello M (2002) Escaping free-energy minima. *Proceedings of the National Academy of Sciences* 99: 12562–12566.
- Landau LD and Lifshitz EM (1980) *Statistical Physics. Part I.* (Course of Theoretical Physics, v. 5), 3rd edn., 544 pp. Oxford: Butterworth and Heinemann.
- Legrand B (1984) Relations entre la structure électronique et la facilité de glissement dans les métaux hexagonaux compacts. *Philosophical Magazine* 49: 171–184.
- Lin JF, Struzhkin VV, Jacobsen SD, et al. (2005) Spin transition of iron in magnesiowustite in Earth's lower mantle. *Nature* 436: 377–380.

- Liu L-G and Bassett WA (1986) *Elements, Oxides, and Silicates. High-Pressure Phases with Implications for the Earth's Interior*, 250 pp. New York: Oxford University Press.
- Loubeyre P, LeToullec R, Hausermann D, *et al.* (1996) X-ray diffraction and equation of state of hydrogen at megabar pressures. *Nature* 383: 702–704.
- Matsui M (1989) Molecular dynamics study of the structural and thermodynamic properties of MgO crystal with quantum correction. *Journal of Chemical Physics* 91: 489–494.
- McNeil LE and Grimsditch M (1991) Pressure-amorphized SiO₂ α -Quartz: An anisotropic amorphous solid. *Physical Review Letters* 68: 83–85.
- Mishima O, Calvert LD, and Whalley E (1984) Melting of ice I at 77 K and 10 kbar: A new method for making amorphous solids. *Nature* 310: 393–394.
- Montagner J-P and Nataf H-C (1986) A simple method for inverting the azimuthal anisotropy of surface waves. *Journal of Geophysical Research* 91: 511–520.
- Montroll EW (1942) Frequency spectrum of crystalline solids. *Journal of Chemical Physics* 10: 218–229.
- Montroll EW (1943) Frequency spectrum of crystalline solids. II: General theory and applications to simple cubic lattices. *Journal of Chemical Physics* 10: 481–495.
- Murakami M, Hirose K, Kawamura K, Sata N, and Ohishi Y (2004) Post-perovskite phase transition in MgSiO₃. *Science* 304: 855–858.
- Nye JF (1998) *Physical Properties of Crystals. Their Representation by Tensors and Matrices*, 329 pp. Oxford: Oxford University Press.
- Oganov AR and Dorogokupets PI (2003) All-electron and pseudopotential study of MgO: Equation of state, anharmonicity, and stability. *Physical Review B* 67: (art. 224110).
- Oganov AR and Dorogokupets PI (2004) Intrinsic anharmonicity in thermodynamics and equations of state of solids. *Journal of Physics – Condensed Matter* 16: 1351–1360.
- Oganov AR (2002) *Computer Simulation Studies of Minerals*, 290 pp. PhD Thesis, University of London.
- Oganov AR, Brodholt JP, and Price GD (2000) Comparative study of quasi-harmonic lattice dynamics, molecular dynamics and Debye model in application to MgSiO₃ perovskite. *Physics of the Earth and Planetary Interiors* 122: 277–288.
- Oganov AR, Brodholt JP, and Price GD (2001a) The elastic constants of MgSiO₃ perovskite at pressures and temperatures of the Earth's mantle. *Nature* 411: 934–937.
- Oganov AR, Brodholt JP, and Price GD (2002) *Ab initio* theory of thermoelasticity and phase transitions in minerals. In: Gramaccioli CM (ed.) *EMU Notes in Mineralogy, Vol. 4: Energy Modeling in Minerals*, pp. 83–170. Bolin: Springer.
- Oganov AR, Gillan MJ, and Price GD (2003) *Ab initio* lattice dynamics and structural stability of MgO. *Journal of Chemical Physics* 118: 10174–10182.
- Oganov AR, Gillan MJ, and Price GD (2005a) Structural stability of silica at high pressures and temperatures. *Physical Review B* 71: (art. 064104).
- Oganov AR, Martoňák R, Laio A, Raiteri P, and Parrinello M (2005b) Anisotropy of Earth's D'' layer and stacking faults in the MgSiO₃ post-perovskite phase. *Nature* 438: 1142–1144.
- Oganov AR and Ono S (2004) Theoretical and experimental evidence for a post-perovskite phase of MgSiO₃ in Earth's D'' layer. *Nature* 430: 445–448.
- Oganov AR and Ono S (2005) The high-pressure phase of alumina and implications for Earth's D'' layer. *Proceedings of the National Academy of Sciences* 102: 10828–10831.
- Oganov AR and Price GD (2005) *Ab initio* thermodynamics of MgSiO₃ perovskite at high pressures and temperatures. *Journals of Chemical Physics* 122: (art. 124501).
- Oganov AR, Price GD, and Brodholt JP (2001b) Theoretical investigation of metastable Al₂SiO₅ polymorphs. *Acta Crystallographica A* 57: 548–557.
- Parker SC and Price GD (1989) Computer modelling of phase transitions in minerals. *Advances in Solid State Chemistry* 1: 295–327.
- Poirier JP (1999) Equations of state. In: Wright K and Catlow R (eds.) *Miscroscopic Properties and Processes in Minerals*, NATO Science Series, v. C543, pp. 19–42. Dordrecht: Kluwer.
- Poirier J-P (2000) *Introduction to the Physics of the Earth's Interior* 2nd edn. 326 pp. Cambridge: Cambridge University Press.
- Poirier J-P and Price GD (1999) Primary slip system of ϵ -iron and anisotropy of the Earth's inner core. *Physics of the Earth and Planetary Interiors* 110: 147–156.
- Price GD and Yeomans J (1984) The application of the ANNNI model to polytypic behavior. *Acta Crystallographica B* 40: 448–454.
- Price GD (1983) Polytypism and the factors determining the stability of spinelloid structures. *Physics and Chemistry of Minerals* 10: 77–83.
- Rao CNR and Rao KJ (1978) *Phase Transitions in Solids: An Approach to the Study of the Chemistry and Physics of Solids*, 330 pp. NY: McGraw-Hill.
- Redfern SAT (2000) Order-disorder phase transitions. *Reviews in Mineralogy and Geochemistry* 39: 105–133.
- Richet P and Gillet P (1997) Pressure-induced amorphisation of minerals: A review. *European Journal of Mineralogy* 9: 907–933.
- Ringwood AE (1991) Phase transformations and their bearing on the constitution and dynamics of the mantle. *Geochimica et Cosmochimica Acta* 55: 2083–2110.
- Robie RA and Edwards JL (1966) Some Debye temperatures from single crystal elastic constant data. *Journal of Applied Physics* 37: 2659–2663.
- Rydberg VR (1932) Graphische Darstellung einiger bandenspektroskopischer Ergebnisse. *Journal of Applied Physics* 73: 376–385.
- Schilling FR, Sinogeikin SV, and Bass JD (2003) Single-crystal elastic properties of lawsonite and their variation with temperature. *Physics of the Earth and Planetary Interiors* 136: 107–118.
- Seitz F (1949) *Modern Theory of Solids*, 736 pp. Moscow: GITTI (Russian translation).
- Shannon RD and Prewitt CT (1969) Effective ionic radii in oxides and fluorides. *Acta Crystallographica B* 25: 925–946.
- Sharma SM and Sikka SK (1996) Pressure-induced amorphization of materials. *Progress in Materials Science* 40: 1–77.
- Sirotni Yu I and Shaskolskaya MP (1975) *Fundamentals of Crystal Physics*, 680 pp. Moscow: Nauka (in Russian).
- Sposito G (1974) Landau's choice of the critical-point exponent β . *American Journal of Physics* 42: 1119–1121.
- Sturhahn W, Jackson JM, and Lin J-F (2005) The spin state of iron in minerals of Earth's lower mantle. *Geophysical Research Letters* 32: L12307.
- Sutton AP (1993) *Electronic Structure of Materials*, 260 pp. Oxford: Oxford University Press.
- Terhune RW, Kushida T, and Ford GW (1985) Soft acoustic modes in trigonal crystals. *Physical Review B* 32: 8416–8419.
- Tröster A, Schranz W, and Miletich R (2002) How to couple Landau theory to an equation of state. *Physical Review Letters* 88: art. 055503.
- Tse JS and Klug DD (1993) Anisotropy in the structure of pressure-induced disordered solids. *Physical Review Letters* 70: 174–177.
- Tsuchiya T, Tsuchiya J, Umemoto K, and Wentzcovitch RM (2004) Phase transition in MgSiO₃ perovskite in the earth's lower mantle. *Earth and Planetary Science Letters* 224: 241–248.

- Umemoto K, Wentzcovitch RM, and Allen PB (2006) Dissociation of MgSiO_3 in the cores of gas giants and terrestrial exoplanets. *Science* 311: 983–986.
- Vinet P, Ferrante J, Smith JR, and Rose JH (1986) A universal equation of state for solids. *Journal of Physics* C19: L467–L473.
- Vinet P, Rose JH, Ferrante J, and Smith JR (1989) Universal features of the equation of state of solids. *Journal of Physics – Condensed Matter* 1: 1941–1963.
- Vočadlo L, Price GD, and Poirier J-P (2000) Grüneisen parameters and isothermal equations of state. *American Mineralogist* 85: 390–395.
- Vorob'ev VS (1996) On model description of the crystalline and liquid states. *Teplofizika Vysokih Temperatur (High-Temperature Thermophysics)* 34: 397–406 (in Russian).
- Wallace DC (1998) *Thermodynamics of Crystals*, 484 pp. New York: Dover Publications.
- Wang Y, Li J, Yip S, Phillpot S, and Wolf D (1995) Mechanical instabilities of homogeneous crystals. *Physical Review B* 52: 12627–12635.
- Wang Y, Yip S, Phillpot S, and Wolf D (1993) Crystal instabilities at finite strain. *Physical Review Letters* 71: 4182–4185.
- Warren MC, Dove MT, Myers ER, *et al.* (2001) Monte Carlo methods for the study of cation ordering in minerals. *Mineralogical Magazine* 65: 221–248.
- Watt JP, Davies GF, and O'Connell RJ (1976) The elastic properties of composite materials. *Reviews of Geophysics and Space Physics* 14: 541–563.
- Welch DO, Dienes GJ, and Paskin A (1978) A molecular dynamical study of the equation of state of solids at high temperature and pressure. *Journal of Physics and Chemistry of Solids* 39: 589–603.
- Wilson KG (1983) The renormalization group and related phenomena. *Reviews of Modern Physics* 55: 583–600.
- Wookey J, Kendall J-M, and Rumpker G (2005) Lowermost mantle anisotropy beneath the north Pacific from differential S-ScS splitting. *Geophysical Journal International* 161: 829–838.
- Yeomans JM (1992) *Statistical Mechanics of Phase Transitions*, 168 pp. Oxford: Oxford University Press.
- Zhang L, Ahsbahs H, Kutoglu A, and Hafner SS (1992) Compressibility of grunerite. *American Mineralogist* 77: 480–483.
- Zharkov VN and Kalinin VA (1971) *Equations of state of solids at high pressures and temperatures*, 257 pp. New York: Consultants Bureau.